Chemical Geology 524 (2019) 329–344

Contents lists available at ScienceDirect

Chemical Geology

journal homepage: www.elsevier.com/locate/chemgeo

Origin of strontium and calcium in pedogenic needle fibre calcite (NFC)

Millière L.[a,b], Gussone N.[a,*], Moritz T.[a], Bindschedler S.[c], Verrecchia E.P.[b]

[a] Institut für Mineralogie, Universität Münster, Corrensstraße 24, D-48149 Münster, Germany
[b] Institute of Earth Surface Dynamics, Faculty of the Geosciences and the Environment, University of Lausanne, Geopolis Campus, CH-1015 Lausanne, Switzerland
[c] Laboratory of Microbiology, Institute of Biology, Faculty of Sciences, University of Neuchâtel, Rue Emile Argand 11, CH-2000 Neuchâtel, Switzerland

ARTICLE INFO

Keywords:
Needle fibre calcite
Soil carbonate
Sr isotopes
Ca isotopes
Fungi

ABSTRACT

Strontium (Sr) and calcium (Ca) isotopic compositions and Sr/Ca ratios have been analysed in different fractions of pedogenic needle fibre calcite (NFC) from the Swiss Jura Mountains (Villiers, Neuchâtel, Switzerland) in order to determine their Ca sources and to investigate the potential role of fungi in the origin of NFC. $^{87}Sr/^{86}Sr$ ratios have been measured to trace the Ca trapped within different pedogenic carbonate. This ratio was compared for previously identified microscopic morphological groups of NFC, the bulk soil fine earth (< 2 mm), the carbonate host rock (CHR), a late calcitic cement (LCC, another pedogenic carbonate precipitated physicochemically at the same depth as NFC in soil pores), the soil solution, and the throughfall. The $^{87}Sr/^{86}Sr$ indicated a mixing of weathered allochthonous minerals (an atmospheric component) and the dissolved CHR (the local geogenic component). Moreover, the comparison of $^{87}Sr/^{86}Sr$ ratios of the different types of NFC with LCC suggests that the contribution of Ca from the main Ca sources slightly differs between NFC morphotypes and LCC. In addition, the three NFC morphotypes displayed Sr isotopic compositions different from each other, emphasizing a direct relationship between the microscopic shapes of NFC and the processes involved in their respective formation, including the origin of the Ca. Strontium concentrations and $\delta^{44/40}Ca$ values of NFC and LCC crystals were used to determine possible differences in their growth rate and/or micro-environmental conditions during their formation. Crystals described micromorphologically as simple needles (SN) were enriched in ^{44}Ca and depleted in Sr compared to LCC, suggesting that the elongated shape of the SN crystal cannot be related to a rapid precipitation rate, but rather to a slow precipitation. Calculations applied to the soil solution evolution during calcite precipitation demonstrates the utilisation of large portions of the Ca pool for NFC formation within a closed system, e.g. inside an organic mould, such as fungal hyphae. The differences between the three microscopic groups can be explained by a mixing of the SN with a LCC-like compound originating from the soil solution.

1. Introduction

Needle fibre calcite (NFC) is a habitus of calcium carbonate ($CaCO_3$) frequently observed in environments affected by pedogenic processes (Durand et al., 2018) as well as in caves as a component of moonmilk (Borsato et al., 2000; Cañaveras et al., 2006). This study, only dealing with NFC precipitated in soils, is based on “cotton ball”-like NFC and white, consolidated (but still plastic) coatings attached to soil grains (Jones and Kahle, 1993; Verrecchia and Verrecchia, 1994; Cailleau et al., 2009a; Millière et al., 2011a, 2011b). NFC is a monocrystal in the shape of a needle with an average diameter of 1–2 μm and a length reaching 10^2 times its width. Microscopically, there is a high variability in morphologies (Cailleau et al., 2009a). Three main microscopic groups have been identified in the Swiss Jura Mountains: simple needle (SN), simple needles with calcitic overgrowths (SNO), and simple needles with nanofibres (SNN; Millière et al., 2011a); nanofibres consist of nano-sized needle-like crystals or organic matter (Bindschedler et al., 2014). According to previous studies, simple needles correspond to the original form of NFC, which can evolve into the two other microscopic morphologies inside the soil pore space (Vergès et al., 1982; Verrecchia and Verrecchia, 1994; Cailleau et al., 2009a; Millière et al., 2011a). Nevertheless, despite intense work on NFC, its origin and the processes involved in its formation are still under debate. Since NFC has never been reproduced in the laboratory, processes leading to the precipitation of calcite in such an elongated shape with its particular crystallographic properties are still unexplained (Iwanoff, 1906; Mügge, 1914; Stoops, 1976 and Vergès et al., 1982). Morphological similarities between fungal hyphae and simple needles of calcite observed in soils

* Corresponding author.
E-mail address: nikolaus.gussone@wwu.de (N. Gussone).

https://doi.org/10.1016/j.chemgeo.2019.06.022
Received 28 March 2019; Received in revised form 19 June 2019; Accepted 22 June 2019
Available online 26 June 2019

Abbreviations

CHR	carbonate host rock
$\delta^{44/40}Ca$	$= (((^{44}Ca/^{40}Ca)_{sample}/(^{44}Ca/^{40}Ca)_{SRM915a} - 1) * 1000$.
DSS	deep soil solution
NFC	needle fibre calcite
LCC	late calcitic cement
SN	simple needle morphology
SNN	simple needle covered by nanofibres
SNO	simple needle with calcite overgrowth

(Callot et al., 1985a, 1985b; Phillips and Self, 1987; Verrecchia and Verrecchia, 1994; Bindschedler et al., 2012) led authors to propose that NFC could precipitate inside organic structures acting as moulds, constraining calcite crystals to grow in the shape of a needle along an axis other than their *c* axis. The different NFC morphotypes, and a late calcitic cement (LCC) from the same soil depth, have been sampled in the Swiss Jura Mountains (Villiers quarry). Their oxygen and carbon isotope ratios are similar, suggesting precipitation in the same environmental conditions (e.g. temperature; Millière et al., 2011a). Thus, the growth of NFC crystals inside fungal hyphae is currently the favoured hypothesis, which is consistent with the formation of elongated crystals of NFC in isotopic equilibrium with its local environment.

The understanding of soil carbonate formation and the incorporation of geochemical tracers have wide implications for environmental studies. For instance, the formation of soil carbonate in epi-karst can influence the chemistry of cave deposits, which are frequently used archives as well as by the reconstruction of paleo-climate directly based on soil carbonate, e.g. in loess (Li et al., 2013; Li et al., 2017).

Strontium (Sr) is currently used as a tracer of calcium (Ca), as it is accepted that $^{87}Sr/^{86}Sr$ incorporation into carbonate is not affected by growth conditions, such as the temperature or the growth rate (Capo et al., 1998). Strontium isotope composition allows the two main sources of Ca to be traced in a soil system, namely Ca released from minerals present in the soil and the parent rock on one hand, and the atmospheric contribution through dusts and rainfall inputs, on the other hand. If external (atmospheric input) and in situ (local mineral weathering) sources of Sr in the soil have different $^{87}Sr/^{86}Sr$ ratios, they can be used to trace the origin of Sr, and thus, those of Ca entrapped into pedogenic secondary $CaCO_3$ (Graustein and Armstrong, 1983; Capo and Chadwick, 1999; Quade et al., 1995; Capo et al., 1998; Chiquet et al., 1999; Naiman et al., 2000; Van der Hoven and Quade, 2002).

The total Sr concentration in a calcite crystal is complementary to the approach by Sr isotopic composition, as it gives some information on the chemical environment, which influences the amount of minor and trace elements incorporated in the calcium carbonate crystal during its growth. Several variables influence Sr partitioning in calcite crystals (McIntire, 1963; Morse and Bender, 1990). Strontium incorporation into biogenic and inorganic calcite may increase with the increasing calcification and precipitation rate, respectively (Lorens, 1981; Tesoriero and Pankow, 1996; Lea et al., 1999; Stoll and Schrag, 2000; Huang and Fairchild, 2001; Stoll et al., 2002a, 2002b; Wasylenki et al., 2005; Nielsen et al., 2013; Gabitov et al., 2014). A negative temperature dependence for Sr has also been demonstrated in inorganic calcite (Holland et al., 1964; Kinsman, 1969), whereas in biogenic calcite precipitation experiments, the Sr temperature dependence is still poorly understood (Katz et al., 1972; Lea et al., 1999; Humphrey and Howell, 1999; Malone and Baker, 1999; Stoll et al., 2002a, 2002b; Langer et al., 2006).

Another tool used to study $CaCO_3$ precipitation processes is the stable isotopic composition of Ca ($\delta^{44/40}Ca$). Although the exact mechanisms of Ca fractionation during calcite precipitation are still under discussion, the Ca isotopic composition has been suggested as a valuable tool for constraining processes during $CaCO_3$ formation (Schmitt et al., 2018; Moynier and Fujii, 2017; Gussone et al., 2016). Factors that have been shown to influence the $\delta^{44/40}Ca - *$ of a $CaCO_3$ mineral are (i) temperature (Gussone et al., 2003; Marriott et al., 2004), (ii) precipitation rate (Lemarchand et al., 2004; Tang et al., 2008b), (iii) solution stoichiometry (Nielsen et al., 2012), (iv) crystal structure (Gussone et al., 2005, 2011) and (v) reservoir utilisation (Rayleigh-type fractionation, Teichert et al., 2005).

The objectives of this study were two-folds. First, by using the $^{87}Sr/^{86}Sr$ ratio, it aimed at quantifying the contribution of different Ca sources in the various $CaCO_3$ deposits found at the Villiers quarry (CHR – carbonate host rock, LCC, and the three microscopic morphological groups of NFC), as well as in soil leachates and one sample of rainwater. The different $CaCO_3$ deposits were precipitated in the same environment, but likely by different processes. Therefore, determining whether the Ca constituting the NFC originates from the carbonate host rock (CHR) or from atmospheric inputs, in a context of high atmospheric precipitations (rainfalls and snowfalls), represents a clue for their origin. In addition to this, since pedogenic carbonates can act as an atmospheric carbon sink in the Jura Mountains (e.g. Hasinger et al., 2015), the $^{87}Sr/^{86}Sr$ ratio can be used to quantify the contribution of each source for the Ca entrapped within NFC and LCC crystals. The second objective of this study was to better understand the conditions that led to the precipitation of the three microscopic morphologies of NFC, as well as of the LCC. For this, the $\delta^{44/40}Ca$ values and Sr/Ca ratios were determined on $CaCO_3$ and soil solution samples harvested at regular intervals. These results allowed discussing the potential genetic relationships between the three microscopic morphological groups and hence the origin of NFC.

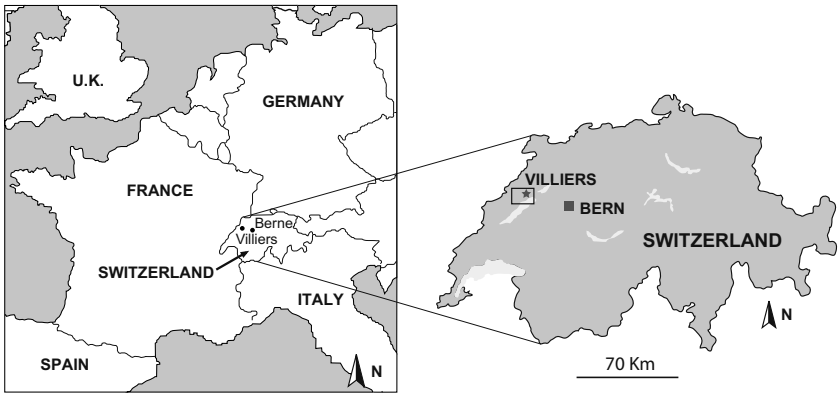

Fig. 1. Geographical location of the studied area in western Europe and Switzerland.

2. Site description

The study area (Villiers quarry, 47°04′N, 6°59′E, 769 m a.s.l.) is situated in the Swiss Jura Mountains, approximately 15 km NNE from the city of Neuchâtel, and about 60 km from Bern (Fig. 1). Climate data recorded in this region report a mean annual rainfall of 1200 mm and a mean annual temperature of 6 °C. Periodically, air masses from the Western Sahara, Moroccan Atlas, and central Algeria transport dust that falls down over western Europe (Middleton and Goudie, 2001), contributing to the geochemistry of pedogenic processes. Finally, the area is affected by a succession of anticlines and synclines deforming the geological substratum composed of Jurassic and Cretaceous limestones.

The studied soil is located near a quarry, at the foot of an anticline affected by two overthrusts (Burkhard and Sommaruga, 1998). This calcareous soil in Villiers is developed on indurated scree deposits, mainly formed during the Last Glaciation (Würm; Arn, 1992) by freezing and shattering of the superficial part of the parent limestone. Pores and cracks between cryoclasts are filled with vadose silt formed by a mixing of fragments of recrystallized Mesozoic limestone, iron oxyhydroxides, clays, quartz and mica grains (Fig. 2). Pochon (1978) has demonstrated that the main part of the mineral fraction forming soils in the Swiss Jura Mountains is aeolian in origin. Later on, during the Holocene, vegetation growth on scree slope deposits contributed to the incorporation of organic matter and the formation of a well-developed soil. The vegetation at the studied site corresponds to a beech and fir trees forest. The soil corresponds to a hypocalcic Calcisol (hyperhumic skeletic) pedon according to the IUSS Working Group WRB (2006). The uppermost horizon, identified as an Aca horizon, is dark brown, indicating a high amount of organic matter. Small calcareous fragments, between 2 and 20 mm, constitute the soil skeleton (coarse fraction). Roots are extremely abundant in this horizon, with a highly developed porosity. No secondary carbonate has been observed in the Aca horizon. The Bcah horizon, between 20 and 60 cm deep, is characterised by a large amount of organic matter and is also dark brown. The limit between the two uppermost horizons is sharp. The calcitic skeleton is also extremely abundant, and the size of cryoclasts and rock fragments ranges from 2 to 50 mm. NFC is observed in the deepest part of the Bcah horizon. Finally, the deepest horizon is a Ccak. The coarse skeleton, formed by calcareous cryoclasts, is covered with or embedded in secondary $CaCO_3$. This horizon is characterised by a high porosity and an intense drainage down to a depth of 60 cm. The size of cryoclasts mostly varies between 10 mm and 10 cm, roots are abundant, as well as fungal rhizomorphs. The limits between the upper (Aca and Bcah) and mineral horizons (Cca) are sharp and undulated (Fig. 2).

3. Methods

3.1. Sample collection

3.1.1. Sampling scheme to inventory Sr and Ca in different soil and $CaCO_3$ compartments

In order to identify the sources of Ca in the various $CaCO_3$ compartments at the Villers quarry several samples have been harvested. Carbonate host rock samples (CHR; $n = 5$) were randomly sampled in various locations at the base of the quarry, as well as in the soil profile, in order to have a wide range of $^{87}Sr/^{86}Sr$ values of this potential Ca source (i.e. the carbonate host rock). The late calcite cement (LCC; $n = 7$) was sampled in highly cemented blocky cryoclasts forming the lowest part of the soil. 17 samples of two macroscopic morphologies of NFC ("cotton ball"-like aggregates and white coatings) were selectively collected in the soil profile (between 60 and 130 cm deep) with polypropylene tweezers. Sampling of these two macroscopic shapes of NFC

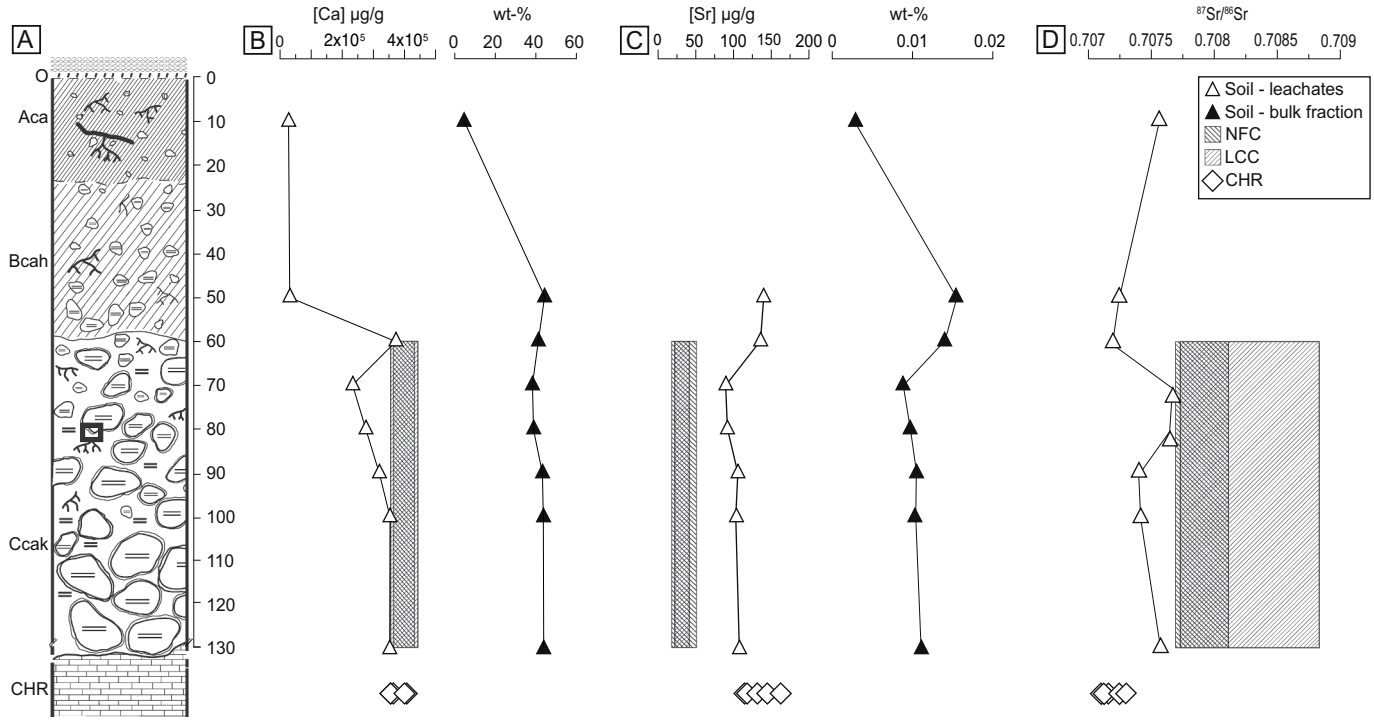

Fig. 2. Sketch and chemical characteristics of the soil profile at Villiers. (A) Soil profile at Villiers quarry. The soil is divided into three main horizons: the Aca, rich in organic matter, the (Bcah), depleted in $CaCO_3$ but still enriched in organic matter, and the Ccak horizon composed of calcareous scree deposits, enriched in needle fibre calcite (NFC) in pores between the cryoclasts, and partly cemented by secondary calcium carbonate (LCC). (B) Ca concentrations in NFC and LCC (shaded areas), carbonate host rock (CHR, lozenges) in ppm and soil (triangles). White triangles represent Ca concentrations in ppm of soil leachates, black triangles those of the total soil powder, given as weight percent (wt%). (C) Sr concentrations in NFC and LCC (shaded areas), CHR (lozenges) in ppm and soil. White triangles represent Sr concentrations in ppm of soil leachates and black triangles the Sr concentration for the total soil powder given in weight percent (wt%). (D) Strontium isotope signature of soil leachates, NFC, CHR, and LCC. Each value is plotted according to the depth. The box in bold drawn in the soil sketch at 80 cm deep shows the place where thin sections of Fig. 6 have been sampled.

was carried out randomly from August 2006 to October 2009. The top soil layer was sampled within the uppermost 10 cm and then, the deeper soil material each 10 cm, starting from 50 to 100 cm deep in the soil profile, where the NFC is most abundant. The samples were collected and stored in polypropylene boxes, which were previously washed with 10% nitric acid (HNO_3) in a sonic bath for 1 h and then rinsed twice with deionised water. Finally, the soil percolating solutions (soil leachates) were sampled in free lysimeters at two different depths: 40 and 110 cm, both on two dates, February the 25th 2008 and April the 25th 2008, which corresponds to the gathering of soil solutions from January the 15th 2008 to February the 25th 2008, and from February the 25th 2008 to April the 24th 2008, respectively. The conventional total alkalinity (mainly as CO_3^{2-}) of the soil percolating solutions ranged from 1.26 mmol/L to 2.40 mmol/L. The rainwater was collected on February the 25th 2008 in polypropylene tubs placed in a box on a tree stump in order to avoid possible contamination due to the "splash" effect (Schultz et al., 1985) and corresponds to the same time period as the percolating water sampled on February the 25th 2008. Rainwater has been collected under the forest cover and is thus qualified as "throughfall".

3.1.2. Seasonal sampling experiment

In order to get Ca and Sr geochemical signatures through different seasons, the soil water (leachates) and the different morphotypes of NFC samples have been harvested monthly (between September 2013 and May 2014) at Villiers, as the site provided large quantities of NFC, in order to get geochemical signatures through different seasons. The periodically sampled site was the same as the one that was monitored during a previous study devoted to the measurements of carbon and oxygen isotopes' variability (Millière et al., 2011a, 2011b; Hasinger et al., 2015). Unfortunately, because the Villiers quarry was still exploited between the sampling sessions (beginning of September and October 2013), the quarry has been partially refilled, making further regular sampling at the same depth and location impossible. For the same reasons, the cleaning of the sampling areas (by removing the already formed NFC in order to obtain only new formed ones) was not effective for the entire period, since the pre-cleaned areas have been recovered by quarry material. Therefore, from October 2013 to May 2014, the sampling was carried out in another place of the quarry wall, cleared a few meters up to an equivalent location of the previous sampling area. During this period, the two NFC morphotypes, i.e. cotton ball-like structures of NFC and NFC coatings on pebbles, have been sampled at each sampling session, along with late calcitic cements (LCC), the soil solution, and the rainwater, when available. Finally, the soil solution (leachates) has been sampled in lysimeters buried in the wall profile, a few centimetres above the NFC accumulations.

3.2. Sample preparation

The different NFC samples (SN, SNO, and SNN) were sorted under a binocular microscope in order to remove organic matter and any other possible contaminant material. The carbonate host rock (CHR) and the late calcitic cement (LCC) were sawed in the laboratory in order to eliminate potential surficial alteration and then crushed in an agate mortar. The soil samples were air-dried, sieved at 2 mm, and the fraction < 2 mm has been crushed, corresponding to the fine earth fraction. Part of the powder was used for the measurements of Sr and Ca isotope compositions (see below) and the other part was used to make pressed chips to perform analyses of element concentrations.

3.2.1. Strontium isotopes

250 mg of each soil sample were dissolved in a closed Savilex Teflon vessel with 10 mL of 7 M HNO_3 acid (suprapur, Merck). Samples were digested in a microwave oven (MSL-Ethos plus, Milestone) using the heating program of the EPA 3051 method (20 min at 175 °C ± 5 °C). After cooling down, the solution was filtered on a cellulose acetate filter (0.45 µm) in order to remove undissolved particles. Soil solution samples were filtered through a 0.2 µm cellulose acetate filter and acidified with 7 M HNO_3 (suprapur, Merck) before evaporation. Each carbonate phase (CHR, LCC, SN, SNO, and SNN) was acidified with 7 M HNO_3 (ultrapur, Merck) in a Teflon vessel and evaporated at 120 °C, whereas the soil solution and soil samples in solution were directly evaporated. The evaporation residues were collected in 0.5 mL 1 M HNO_3. Strontium was concentrated and solutions purified by a passage through cation exchange columns containing Sr-Spec® resin (Waight et al., 2002).

3.2.2. Calcium isotopes

Powders of carbonate samples (LCC, CHR, SN, SNO, and SNN) were loaded into Teflon screw top vials, weighted, and dissolved in 2.5 N HCl. Aliquots of the sample digest were mixed with a ^{42}Ca-^{43}Ca-doublespike (Gussone et al., 2010, 2011) to correct for isotope fractionation during data acquisition in the mass spectrometer. The spike sample mixture was dried and recovered in 6 N HCl. Soil samples and throughfall waters were mixed with a ^{42}Ca-^{43}Ca-double-spike, dried down and recovered in 1.8 N HCl. Calcium was isolated using a 100 µL column volume HCl-chemistry with MCI Gel CK08P (75–100 µm) (Teichert et al., 2009; Ockert et al., 2013). The purified Ca solution was dried down and recovered in 6 N HCl.

3.3. Analytical methods

3.3.1. Strontium isotopes

Strontium isotope ratios were measured at the University of Bern (Switzerland) using a Nu-instruments® Multicollector Inductively Coupled Plasma Mass Spectrometer (MC-ICP-MS). The reproducibility of the $^{87}Sr/^{86}Sr$ measurements was estimated by repeated analyses of the NBS 987 Sr standard, which were statistically undistinguishable, with a mean value of 0.710183 ± 0.000012 (2σ, $n = 9$).

3.3.2. Calcium isotopes

About 300 ng Ca was loaded on outgassed Re-single filaments using the sandwich technique (TaF_5-solution - sample - TaF_5-solution). The Ca isotope composition was determined by thermal ionization mass spectrometry on a Thermo Fisher Scientific Triton thermal ionization mass spectrometer at the Institut für Mineralogie, Universität Münster (Germany). Measurements were performed in static mode, simultaneously measuring ^{40}Ca, ^{42}Ca, ^{43}Ca, and ^{44}Ca. Potential interference of ^{40}K on ^{40}Ca was monitored on mass ^{41}K, but was always found negligible. Instrumental mass fractionation was corrected by an iterative approach using the routine of Heuser et al. (2002). Calcium isotope ratios are expressed as $\delta^{44/40}Ca$ relative to the NIST SRM 915a standard as follows (Eq. (1)):

$$\delta^{44/40}Ca\ [‰] = \left(\frac{\left(\frac{^{44}Ca}{^{40}Ca}\right)_{\text{sample}}}{\left(\frac{^{44}Ca}{^{40}Ca}\right)_{\text{SRM 915a}}} - 1 \right) \times 1000 \quad (1)$$

and average values are calculated as weighted averages. The dolomite standard J-Do gave a $\delta^{44/40}Ca$ value of 0.70‰ ± 0.04‰ ($n = 7$). The twofold standard deviation (2SD) of J-Do measurements was ± 0.07‰, which is consistent with the average 2 SD of replicate sample analyses of < 0.1‰. Analysis of four modern seawater samples (GeoB 9506-4) revealed a $\delta^{44/40}Ca$ of 1.93 (± 0.05‰ 2se; 0.11‰ 2SD), in agreement with published values (e.g. Heuser et al., 2016).

3.3.3. Ca and Sr concentrations

The elemental concentration of the different $CaCO_3$ phases and the soil leachates were analysed by ICP-MS (Thermo Fisher Element XR) at the University of Lausanne (Switzerland). 50 µg of either of the three NFC morphotypes were first dissolved in 0.2 mL of 65% HNO_3

(suprapur, Merck) and then diluted in 0.8 mL of deionised water. 1 mg of LCC or CHR were dissolved in 4 mL of 65% HNO_3 and diluted in 16 mL of deionised water. Calcium and Sr concentrations in soil samples have been analysed with two different methods. First, X-ray fluorescence (XRF) PANanalytical Axios spectrometer was used at the University of Lausanne. The results obtained from X-ray fluorescence (XRF) correspond to the overall elemental content of the solid phases, independently of whether the element is part of a mineral, an amorphous phase, or if it is adsorbed at the surface of a solid (Pfeifer et al., 1991). Second, the total concentration was also determined by an acid extraction method corresponds to 15–85% of the concentration determined by XRF (Meyer, 1991). The acid extraction removes all relatively mobile cations, a method which has led several authors to call the "labile reservoir" the phase resulting from HNO_3 extraction (Chow et al., 1973; Shirahata et al., 1980; Ng and Patterson, 1982; Erel et al., 1990; Steinmann and Stille, 1997; Pourcelot et al., 2008). Thus, the first method is used to measure Ca and Sr concentrations throughout the soil bulk fraction, as it pictures the soil elemental composition; the second method is used to compare Ca and Sr concentrations in soil leachates and carbonate phases.

The Sr/Ca ratio of the soil solution and NFC morphotypes sampled during the seasonal sampling experiment were determined on a Varian Vista Pro Inductively Coupled Plasma Optical Emission Spectrometer (ICP-OES) at the Institut für Mineralogie (University of Münster, Germany), similar to the method described in Gussone and Friedrich (2018), using the following wavelength of 393.366 nm for Ca and 407.771 nm for Sr. Repeated measurements of home standards (coral and artificial solutions) were performed for correction of instrumental drift and day-by-day variations. The analytical uncertainties were determined by replicate measurements of standards and selected samples and were in the range of 0.2 to 0.5 % for Sr/Ca (1 SD). Coral standard JCP-1 revealed Mg/Ca and Sr/Ca ratios of 4.19 and 8.77 mmol/mol, respectively, similar to the values reported by Okai et al. (2004), ranging from 4.16 to 4.18 mmol/mol Mg/Ca, 8.69 to 8.71 mmol/mol Sr/Ca, and within the range of values reported by Hathorne et al. (2013).

3.4. Calculations

The $^{87}Sr/^{86}Sr$ ratios of CHR, LCC, NFC (SN, SNN, SNO microscopic morphotypes), and soil samples were compared using a *t*-test (calculated with Matlab™ software). The SN, SNN, SNO microscopic morphologies were also compared with a statistical *t*-test. The LCC and

Table 1
Values of the $^{87}Sr/^{86}Sr$ ratio, calcium (Ca) and strontium (Sr) concentrations, and calcium isotope compositions of the carbonate host rock (CHR), the late calcitic cement (LCC), the three microscopic morphological groups of needle fibre calcite (NFC), i.e. SN (simple needle), SNN (simple needle with nanofiber) and SNO (simple needle with overgrowths), the soil solution, and the soil fine earth fraction (soil, at various depths in cm) from the inventory sampling.

Sample name	Sample type	$^{87}Sr/^{86}Sr$	[Ca] $\mu g \cdot g^{-1}$	[Sr] $\mu g \cdot g^{-1}$	[Sr/Ca] mol/mol	$\delta^{44/40}$Ca (‰)[a]	2SD[c]
CH01-17B	SN	0.70769 ± 4.6 × 10^{-5}	406,902.0	21.0	2.36 × 10^{-5}	_	
CH01-22	SN	0.70777 ± 7.8 × 10^{-5}	401,814.0	19.6	2.23 × 10^{-5}	0.54	
CH01-24	SN	0.70769 ± 5.6 × 10^{-5}	386,747.0	18.5	2.19 × 10^{-5}	0.66	
CH01-24A	SN	0.70789 ± 6.4 × 10^{-5}	402,857.0	19.3	2.19 × 10^{-5}	0.49	
CH01-30A	SNN	0.70811 ± 4.8 × 10^{-5}	_	_		_	
CH01-30A1	SNN	0.70793 ± 3.4 × 10^{-5}	_	_		_	
CH01-29A	SNN	0.70807 ± 7.6 × 10^{-5}	395,576.0	20.2	2.34 × 10^{-5}	_	
CH01-30B	SNN	0.70797 ± 3.6 × 10^{-5}	384,936.0	23.8	2.83 × 10^{-5}	_	
CH01-03A	SNN	0.70770 ± 4.8 × 10^{-5}	405,843.0	26.5	2.99 × 10^{-5}	_	
CH01-29A1	SNN	0.70796 ± 8.8 × 10^{-5}	395,576.0	20.2	2.34 × 10^{-5}	_	
CH01-01C	SNN	_	393,364.9	21.7	2.52 × 10^{-5}	0.19	0.12
CH01-05	SNN	_	394,051.3	25.3	2.94 × 10^{-5}	0.26	
CH01-24B	SNN	0.70786 ± 9.8 × 10^{-5}	400,290.0	23.2	2.65× 10^{-5}	0.42	
CH01-13	SNO	0.70792 ± 7.6 × 10^{-5}	403,179.0	51.5	5.84 × 10^{-5}	_	
CH01-14	SNO	0.70810 ± 6.0 × 10^{-5}	395,013.0	28.4	3.29 × 10^{-5}	_	
CH01-23	SNO	0.70796 ± 6.6 × 10^{-5}	407,305.0	22.9	2.57 × 10^{-5}	0.37	
CH01-26	SNO	0.70785 ± 4.0 × 10^{-5}	408,982.0	26.5	2.96 × 10^{-5}	0.34	
CH01-28	SNO	0.70794 ± 6.4 × 10^{-5}	409,831.0	40.4	4.51 × 10^{-5}	0.30	
CH01-C1	LCC	0.70814 ± 3.6 × 10^{-5}	392,324.0	31.2	3.64 × 10^{-5}	−0.08	
CH01-C2	LCC	0.70883 ± 2.0 × 10^{-5}	403,615.0	31.6	3.58 × 10^{-5}	−0.36	0.08
CH01-C4	LCC	0.70773 ± 3.8 × 10^{-5}	386,100.0	42.3	5.01 × 10^{-5}	0.03	
CH01-C5	LCC	0.70786 ± 5.4 × 10^{-5}	404,632.0	22.4	2.53 × 10^{-5}	_	
CH01-21B1	LCC	0.70781 ± 5.4 × 10^{-5}	397,666.0	24.5	2.82 × 10^{-5}	_	
CH01-20C	LCC	0.70778 ± 3.6 × 10^{-5}	415,544.0	29.5	3.25 × 10^{-5}	_	
CH01-001	CHR	0.70724 ± 2.4 × 10^{-5}	364,149.0	115	1.44 × 10^{-4}	0.95	0.02
CH01-002	CHR	0.70729 ± 2.4 × 10^{-5}	355,370.0	131	1.69 × 10^{-4}	0.66	
CH01-003	CHR	0.70712 ± 2.6 × 10^{-5}	407,325.0	145	1.63 × 10^{-4}	1.04	
CH01-004	CHR	0.70709 ± 3.6 × 10^{-5}	399,981.0	163	1.86 × 10^{-4}	_	
CH01-005	CHR	0.70715 ± 2.0 × 10^{-5}	355,032.0	144	1.86 × 10^{-4}	_	
Th (25.02)[b]	Throughfalls	0.70757 ± 2.4.10^{-5}	0.5	2.35 × 10^{-4}	2.15 × 10^{-4}	0.35	0.05
SS-50 (25.02)[b]	Soil solution	0.70766 ± 4.0 × 10^{-5}	36.1	7.35 × 10^{-3}	9.31 × 10^{-4}	0.82	0.08
SS-110 (25.02)[b]	Soil solution		35.9	7.64 × 10^{-3}	9.73 × 10^{-4}	0.70	
SS-50 (25.04)[b]	Soil solution		36.6	6.83 × 10^{-3}	8.54 × 10^{-4}	0.62	
SS-110 (25.04)[b]	Soil solution		52.7	9.68 × 10^{-3}	8.40 × 10^{-4}	0.51	
CH01-P10	Soil (10 cm)	0.70756 ± 2.0 × 10^{-5}	27,544.3	_		_	
CH01-P50	Soil (50 cm)	0.70724 ± 2.8 × 10^{-5}	31,771.7	140	2.01 × 10^{-3}	_	
CH01-P60	Soil (60 cm)	0.70719 ± 2.8 × 10^{-5}	372,829.2	136	1.67 × 10^{-4}	_	
CH01-P70	Soil (70 cm)	0.70767 ± 3.6 × 10^{-5}	234,075.8	90	1.76 × 10^{-4}	_	
CH01-P80	Soil (80 cm)	0.70765 ± 3.0 × 10^{-5}	276,334.7	92	1.52 × 10^{-4}	_	
CH01-P90	Soil (90 cm)	0.70740 ± 4.2 × 10^{-5}	319,704.1	106	1.51 × 10^{-4}	_	
CH01-P100	Soil (100 cm)	0.70742 ± 3.0 × 10^{-5}	353,385.9	104	1.34 × 10^{-4}	_	
CH01-P130	Soil (130 cm)	0.70757 ± 2.7 × 10^{-5}	352,416.8	108	1.40 × 10^{-4}	_	

[a] $\delta^{44/40}$Ca values relative to the NIST SRM 915a standard.
[b] Different solutions have been sampled during the year 2008.
[c] $n = 2$. Average 2SD of standards and samples about 0.09‰ applicable for samples analysed once.

NFC samples have been considered as a mixture of two sources: atmospheric input and weathering of the carbonate host rock. Therefore, the proportion of Sr in each sample has been calculated using mixing equation (Eq. (2)) (Capo et al., 1998):

$$X\,(Sr)_{Atm} = \frac{(^{87}Sr/^{86}Sr)_{Cal} - (^{87}Sr/^{86}Sr)_{CHR}}{(^{87}Sr/^{86}Sr)_{Atm} - (^{87}Sr/^{86}Sr)_{CHR}} \quad (2)$$

where X $(Sr)_{Atm}$ represents the mass fraction of Sr derived from atmospheric source. Atm and CHR subscripts refer to the atmospheric and carbonate host rock end-members, respectively. Cal subscript represents the calcite phase (either LCC or NFC morphotypes). The contribution of one of the two end-members to the fraction of calcium can be calculated from the Sr isotope data if the Sr/Ca ratio is known for each component. The relative contribution of atmospheric Ca in the calcite phases can be calculated using the equation (Eq. (3)):

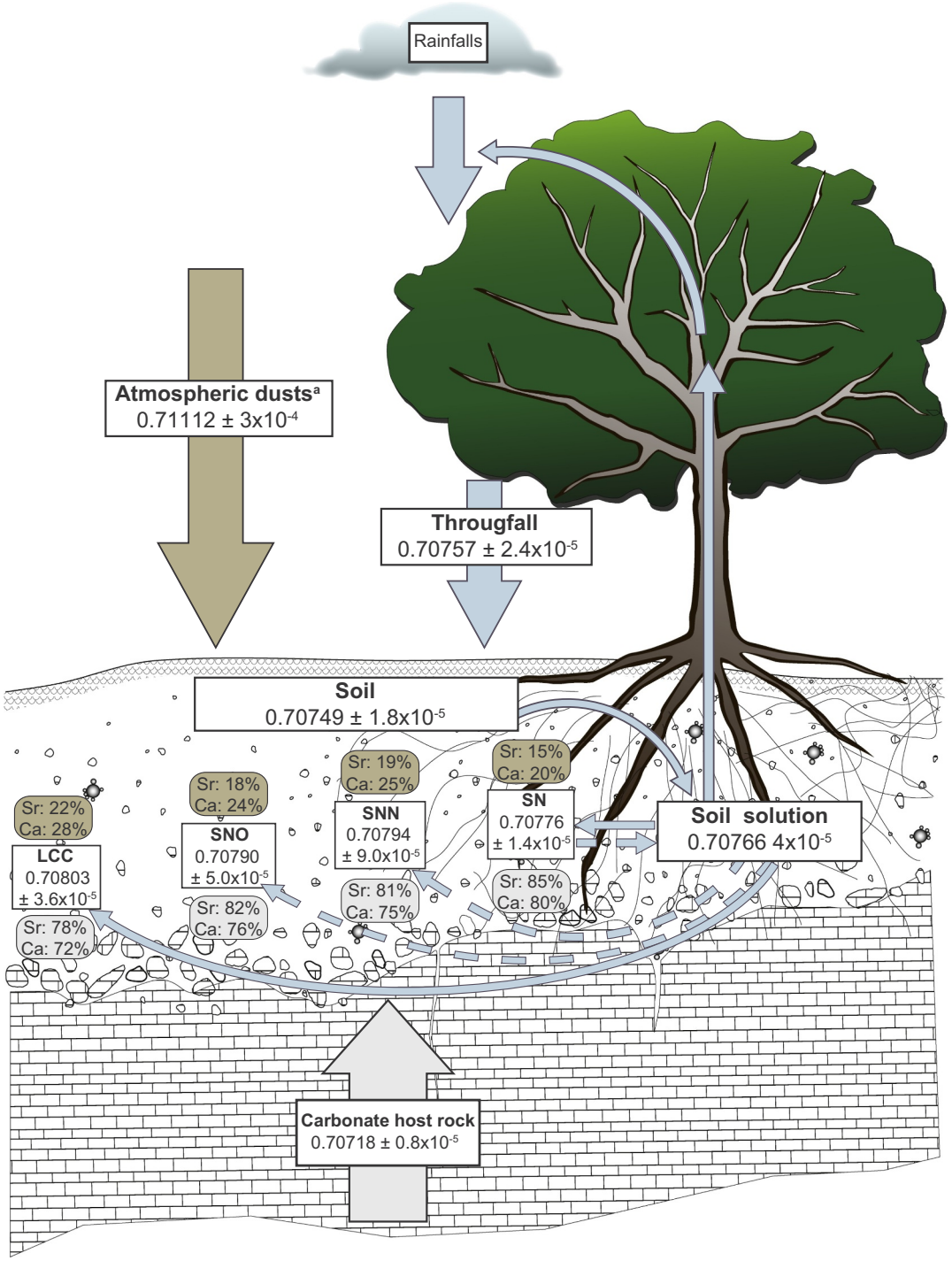

Fig. 3. Average $^{87}Sr/^{86}Sr$ values in the Villiers system. SN: simple needles, SNN: simple needles with nanofibres, SNO: simple needles with overgrowths, LCC: late calcitic cement. Grey arrow and boxes indicate the contribution in calcium and strontium by the carbonate host rock; brown arrow and boxes indicate the input from weathered minerals stemming from the atmospheric dusts. Blue arrows point out the interactions between each component of the ecosystem. [a]: values from Burton et al. (2006). (For interpretation of the references to color in this figure legend, the reader is referred to the web version of this article.)

$$X(Ca)_{Atm} = \frac{\left[\left(\frac{^{87}Sr}{^{86}Sr}\right)_{Cal} - \left(\frac{^{87}Sr}{^{86}Sr}\right)_{CHR}\right] \times \left(\frac{Sr}{Ca}\right)_{CHR}}{\left[\left(\frac{^{87}Sr}{^{86}Sr}\right)_{Cal} - \left(\frac{^{87}Sr}{^{86}Sr}\right)_{CHR}\right] \times \left(\frac{Sr}{Ca}\right)_{CHR} + \left[\left(\frac{^{87}Sr}{^{86}Sr}\right)_{Atm} - \left(\frac{^{87}Sr}{^{86}Sr}\right)_{Cal}\right] \times \left(\frac{Sr}{Ca}\right)_{Atm}} \quad (3)$$

where X $(Ca)_{Atm}$ represents the mass fraction of Ca derived from the atmosphere.

For the calculations, 0.71112 as $^{87}Sr/^{86}Sr_{Atm}$ from Burton et al. (2006) and 1.2×10^{-4} (mol/mol) as $(Sr/Ca)_{Atm}$ from De Angelis and Gaudichet (1991) have been chosen.

4. Results

4.1. Strontium isotopes

The $^{87}Sr/^{86}Sr$ ratios of the CHR (average ± 1 SD; $0.70718 \pm 0.8 \times 10^{-5}$) are in the range of marine carbonate from the Phanerozoic (Table 1) and define the other end-member besides the atmospheric input (see Fig. 3). The $^{87}Sr/^{86}Sr$ ratios of the LCC vary between 0.70773 and 0.70883 (0,70803 ± 4.2×10^{-4}) and they overlap with the $^{87}Sr/^{86}Sr$ ratios of the NFC, which vary between 0.70769 and 0.70811 (0.70793 ± 1.4×10^{-5}). More specifically, the $^{87}Sr/^{86}Sr$ values of the microscopic morphological groups SNO and SNN vary in the same range (SNN: 0.70770 to 0.70811; SNO: 0.70785 to 0.70810) and have similar averages (SNN: 0.70794 ± 5.0×10^{-4}; SNO: 0.70790 ± 9.0×10^{-5}). The simple needle group (SN) has a slightly less radiogenic average value (0.70776 ± 1.4×10^{-4}) compared to the two other microscopic morphological groups and can be statistically differentiated (Fig. 4; Tables 1 and 2). The $^{87}Sr/^{86}Sr$ values of the soil samples from different depths vary between 0.70719 ± 2.8×10^{-5} and 0.70767 ± 3.6×10^{-5}, with an average value of 0.70735 ± 1.8×10^{-5}. The two surficial samples (P-10 and P-50) have the least radiogenic Sr isotope signatures as the values start to increase at 60 cm depth, where the first NFC and LCC occurrences are observed in the soil profile (Fig. 2). Collected throughfall samples and a single soil water sample give $^{87}Sr/^{86}Sr$ ratios of 0.70766 ± 4.0×10^{-5} and 0.70757 ± 2.4×10^{-5}, respectively (Fig. 4, Table 1).

The average of the $^{87}Sr/^{86}Sr$ values of LCC and NFC are statistically different from CHR (Table 2). The average values of the microscopic morphological groups SNN and SNO are statistically indistinguishable but are both different from the SN microscopic group (Table 2). The average LCC $^{87}Sr/^{86}Sr$ ratio is not statistically different from the $^{87}Sr/^{86}Sr$ ratio of the SNN and SNO groups, but distinguishable from the mean $^{87}Sr/^{86}Sr$ ratio of the SN group.

4.2. Strontium and calcium concentrations, $\delta^{44/40}Ca$

Strontium and Ca concentrations and their ratios, as well their respective stable isotopic ratios in the $CaCO_3$ phases, soil samples, and water of the soil inventory are given in Table 1 and in Fig. 2. The $\delta^{44/40}Ca$ and Sr/Ca ratios of the three NFC morphotypes and soil water samples of the seasonal sampling experiment are listed in Table 3. Within the pedogenic $CaCO_3$ fractions, Sr/Ca ratios are on average lowest in SN, intermediate in SNN and SNO and highest in LCC. Calcium concentrations of each phase belong to the same range, showing that samples consist of pure $CaCO_3$, without other carbonate phases or significant contamination by soil particles. In the soil, Ca and Sr concentrations vary as a function of depth and horizon type. Calcium and Sr concentrations in the soil samples increase from 10 cm to 50 cm in depth. Calcium concentrations are stable between 50 cm and 70 cm in depth, while Sr concentrations slightly decrease throughout the same depth interval. From 70 cm downwards, Ca and Sr concentrations are relatively constant (Fig. 2 B, C). Soil solutions (leachates) display Sr and Ca concentrations ranging from 7.35×10^{-3} µg·g^{-1} to 9.68×10^{-3} µg·g^{-1} and from 36.1 to 52.7 µg·g^{-1}, respectively (Table 1 and Fig. 2 B, C). Calcium isotope analyses of CHR, SN, SNN, SNO, LCC, soil water, and throughfall are presented in Tables 1 and 3, as well as in Fig. 5. The average Ca isotope signature of CHR is 0.88‰ and defines the highest end-member value. The average values of Ca isotope composition of the three microscopic shapes of NFC ($\delta^{44/40}Ca_{SN}$ = 0.51‰; $\delta^{44/40}Ca_{SNN}$ = 0.43‰; $\delta^{44/40}Ca_{SNO}$ = 0.27‰) are fairly close to each other, even if the Ca isotope composition of SNO is depleted in ^{44}Ca as compared to the two other microscopic shapes (Fig. 6). The average $\delta^{44/40}Ca$ value of LCC is different from the average $\delta^{44/40}Ca$ values of the three NFC microscopic morphologies, with a mean of −0.01‰. Finally, the average value of the Ca isotope signature of the soil solution ($\delta^{44/40}Ca_{soil\text{-}solution}$ = 0.75‰) is intermediate between the average value of CHR ($\delta^{44}Ca_{CHR}$ = 0.88‰) and throughfall ($\delta^{44/40}Ca_{throughfall}$ = 0.35‰).

5. Discussion

5.1. Sources of Sr and Ca in Villiers quarry

Calcium in soil ecosystems is subject to many exchanges between the soil mineral phases, the soil solution, and the vegetation. The similar chemical behaviour of Sr and Ca allows $^{87}Sr/^{86}Sr$ ratios to be used as a proxy for Ca sources at an ecosystem scale (Poszwa et al., 2000). The radiogenic $^{87}Sr/^{86}Sr$ ratio is not significantly changed during biological processes and mineral precipitation, because all mass-dependent isotope fractionation effects, either of natural origin or taking place during mass-spectrometry and chemical sample treatment, are erased by normalisation to the natural $^{88}Sr/^{86}Sr$ ratio. Thus, the $^{87}Sr/^{86}Sr$ ratio of pedogenic $CaCO_3$ depends only on the mixing between the available sources. When the two main Ca inputs in terrestrial ecosystems, namely the weathering of parent rock as well as the wet and dry atmospheric deposits, are known and sufficiently contrasted, the origin of Ca included in pedogenic $CaCO_3$ can be traced and quantified using mass balance techniques (Capo et al., 1998).

The throughfall samples at Villiers quarry ($^{87}Sr/^{86}Sr$ = 0.70751 ± 2×10^{-5}) are depleted in ^{87}Sr compared to seawater, which is characterised by an extremely uniform global $^{87}Sr/^{86}Sr$ isotope ratio ($^{87}Sr/^{86}Sr$ = 0.70917 ± 1.0×10^{-5}; Dia et al., 1992). This seems to indicate that the wet deposits in Villiers quarry do not, or only partly, originate from seawater. This observation is in line with the statement

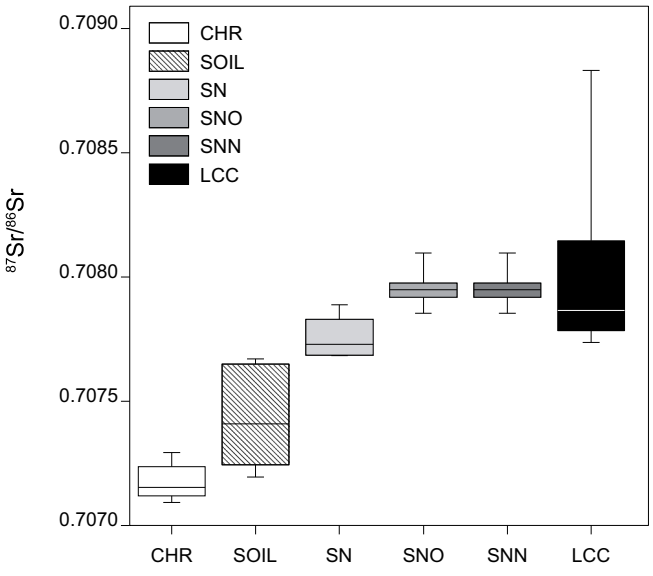

Fig. 4. Box plot showing the $^{87}Sr/^{86}Sr$ ratios of the carbonate host rock (CHR), soil leachates from soil samples (SOIL), the three microscopic morphologies of NFC, i.e. simple needles (SN), simple needles with overgrowths (SNO), simple needles with nanofibres (SNN), and finally, the late calcitic cement (LCC).

Table 2
Statistical *t*-test comparing the mean of the $^{87}Sr/^{86}Sr$ ratio values of the carbonate host rock (CHR), late calcitic cement (LCC) and the three microscopic morphological groups of NFC: simple needle (SN), simple needle with epitactic growth (SNO) and the simple needle with nanofibres (SNN) from the inventory sampling. Significance level $\alpha = 0.05$; n: degree of freedom; hypothesis H1 = different mean; H0 = equal mean.

t-Test on $^{87/86}Sr$	*n*	*p*-Value	Accepted H
CHR/LCC	11	0.0007	H1
CHR/SN	8	$6.99\ 10^{-5}$	H1
CHR/SNO	10	$8.05\ 10^{-8}$	H1
CHR/SNN	11	$2.84\ 10^{-7}$	H1
LCC/SN	10	0.11	H0
LCC/SNO	12	0.59	H0
LCC/SNN	13	0.55	H0
SN/SNO	9	0.013	H1
SN/SNN	10	0.028	H1
SNO/SNN	12	0.82	H0

of Schmitt and Stille (2005) who demonstrated that, following a European west to east cross-section from the Atlantic Ocean to eastern Switzerland, the ocean did not show any clear influence on Ca isotope signatures in rainwater and throughfall. Consequently, Ca present in the atmospheric deposits can originate either from a local source, such as the soil or bedrock erosion close to the studied site, and/or from an external source, such as the erosion of various areas in the region, and/or from exogenic sources, such as weathering products of other continents (Négrel and Roy, 1998; Nakano et al., 2001). At Villiers, the $^{87}Sr/^{86}Sr$ isotope value of the throughfall ($0.70757 \pm 2 \times 10^{-5}$) is close to the average $^{87}Sr/^{86}Sr$ value of the soil parent rock ($[^{87}Sr/^{86}Sr]_{CHR} = 0.70718 \pm 8 \times 10^{-6}$). In the Swiss Jura Mountains, where the quarry of Villiers is located, the bedrock is Jurassic and Cretaceous limestones. Thus, the erosion of the surrounding limestones may contribute significantly to Sr and Ca compositions of the throughfall at Villiers quarry, as it has been demonstrated in other sites (Capo and Chadwick, 1999; Schmitt and Stille, 2005), even if rare rain events can lead to dust deposits from the Sahara (Middleton and Goudie, 2001). Moreover, throughfall results from the wash out of dry atmospheric deposits on leaves and leaf excretions resulting from plant metabolism and evapotranspiration processes (Bailey et al., 1996; Poszwa et al., 2000). The substances and solution excreted by leaves originate from the soil solution, which enters in the roots by suction and circulates through the plant. Despite the fact that vegetation discriminates between Sr and Ca, the $^{87}Sr/^{86}Sr$ values of tree foliage reflects the proportion of each input of Sr, and thus Ca, to the tree (e.g. Miller et al., 1993; Bailey et al., 1996; Blum et al., 2008). At Villiers quarry, the Sr isotope composition of the percolating soil solution is enriched in ^{87}Sr, and could explain the slightly more radiogenic $^{87}Sr/^{86}Sr$ values of the throughfall compared to the CHR. It appears that at Villiers, the throughfall is mainly influenced by two local sources, the surrounding bedrock and, in a minor portion, the soil solution through foliar excretion and leaching.

The hypocalcic Calcisol (hyperhumic skeletic) soil at Villiers is characterised by an abundant skeleton constituted by carbonate scree deposits inherited from the parent rock (Hasinger et al., 2015). Calcium and Sr concentrations (by XRF: black triangles in Fig. 2; by using 1 N HNO_3 acid extraction method: white triangles, Fig. 2) throughout the soil are likely partly influenced by the parent rock, as Ca and Sr are strongly related to carbonate rock sources and both usually show similar behaviours throughout soil profiles (Atteia, 1992; Dalla Piazza, 1996). However, the decrease in Sr concentration between 50 cm and 70 cm deep can be explained by the presence of secondary carbonate at Villiers quarry, i.e. NFC and LCC, which are highly concentrated in Ca but depleted in Sr compared to the CHR (Fig. 2; Table 1). This is confirmed by the Sr isotope composition of $CaCO_3$ phases and soil samples, which are similar between 70 cm and 80 cm in depth, indicating an identical source.

Strontium isotope compositions of all the soil samples, as well as pedogenic $CaCO_3$ accumulations, are enriched in ^{87}Sr compared to CHR, signalling the contribution of another Ca source. The ^{87}Sr enriched sources in general may include phyllosilicates from the host rock and aeolian dust. Micromorphological investigation of soil grains at Villiers allowed clays, quartz, and feldspar to be identified as minerals surrounding calcareous lithoclasts between depths of 60 cm to 100 cm (Fig. 6). A previous study showed that the dissolution of carbonate rocks at the base of soil profiles in the Jura Mountains releases small amounts of phyllosilicates, quartz and feldspar in these calcareous soils (Dalla Piazza, 1996; Martignier and Verrecchia, 2013). Moreover, the identification of plagioclases in soils from the Swiss Jura Mountains in previous studies provides a good indicator of the allochthonous origin of the fine material, as no plagioclase is present in the Jurassic (Jouaffre, 1989) or Cretaceous limestones of this area (Martignier et al., 2013; Martignier et al., 2015). This is also supported by the measurements of higher amounts of quartz and feldspar in the soil than in the rock substratum (Martignier et al., 2013). Finally, in soil samples of this study, quartz grains are small, smooth, and homometric, indicating a possible aeolian origin (Fig. 3; see Martignier et al., 2015). Studies in the Jura Mountains have shown that windblown dust has been contemporaneous to the end of the last glaciation (Würm) during the Late Pleistocene-Holocene transition and has contributed to the pedogenesis of soils in this area during the Holocene (Dalla Piazza, 1996; Martignier et al., 2015). Moreover, other previous studies of soils from different areas developed on calcareous rocks in the Jura Mountains have emphasized a homogeneous geochemistry of the soils, which could be ascribed to aeolian deposits and to the stability of clayey minerals in calcareous environments (Atteia, 1992). This point supports the hypothesis that a non-negligible part of the soil material corresponds to aeolian deposits from the Alps (Pochon, 1978; Martignier et al., 2015). These aeolian deposits, being mainly composed of quartz, K-feldspar and phyllosilicates, with the latter two being enriched in Rb (Capo et al., 1998), contribute to a more radiogenic Sr isotope composition (higher $^{87}Sr/^{86}Sr$).

In addition, Sr isotope compositions of recent atmospheric dust, sampled in ice cores in the Mont Blanc area (French Alps) over the two last centuries, range from 0.7020 to 0.7176 and mainly originate from Saharan dust (Burton et al., 2006). As the Saharan atmospheric dust is known to be transported all over Europe (De Angelis and Gaudichet, 1991; Schwikowski et al., 1995; Burton et al., 2006), it can be assumed that such dust deposit events contributed to the allochthonous minerals observed at Villiers quarry. Several studies have previously shown the importance of the atmospheric input on the amount of Sr and Ca in soils (Graustein and Armstrong, 1983; Capo and Chadwick, 1993; Quade et al., 1995). Consequently, it is likely that the slight enrichment in ^{87}Sr of the soil samples from Villiers results from the mixing of sources issued from the weathering of allochthonous minerals trapped in soils and the dissolution of calcareous parent rocks.

5.2. Sources of calcium in carbonate phases at Villiers quarry

Pedogenic $CaCO_3$ phases at the Villiers quarry are characterised by higher Sr isotope signatures than in the CHR. As explained above, the $^{87}Sr/^{86}Sr$ values of throughfall and CHR measured at Villiers are fairly close to each other. Similar to the soil samples, the high $^{87}Sr/^{86}Sr$ values of LCC and NFC compared to CHR and the throughfall, can be attributed to the weathering and the remobilisation of Sr and Ca present in the allochthonous minerals of the soil. Considering the three NFC morphotypes as a bulk phase, $(^{87}Sr/^{86}Sr)_{NFC}$ values are not statistically different from $(^{87}Sr/^{86}Sr)_{LCC}$ values (Table 2). Nevertheless, calculations to evaluate the contributions of the respective end-members indicate that 85% of the Sr incorporated in NFC originates from the CHR and 15% from allochthonous inputs, and 78% of Sr incorporated in LCC is derived from the CHR and 22% from allochthonous inputs (Fig. 3).

Table 3
$\delta^{44/40}$Ca and Sr/Ca ratios of the three microscopic NFC morphotypes (simple needle (SN), simple needle with epitactic growth (SNO) and the simple needle with nanofibers (SNN)) and soil solutions sampling experiment.

Sample #	Season	type	$\delta^{44/40}$Ca‰	2 SE	2 SD[a]	n	[Ca] ppm	Sr/Ca mol/mol
CH01-102AW1	Summer	Water	0.80	0.06	0.08	2	45.1	2.27E−04
CH01-102AW2	Summer	Water	0.74	0.06	0.08	2	45.6	2.12E−04
CH01-102BW	Summer	Water	0.84	0.07	0.10	2	54.1	2.46E−04
CH01-103EW	Autumn	Water	0.76		0.09	1	69.2	2.26E−04
CH01-104EW1	Autumn	Water	0.71	0.08	0.11	2	60.1	2.09E−04
CH01-104EW2	Autumn	Water	0.80		0.09	1	53.0	2.14E−04
CH01T-106CW	Winter	Water	0.83		0.09	1	25.4	2.28E−04
CH01T-106DW	Winter	Water	0.92	0.08	0.11	2	27.2	2.64E−04
CH01-LCC1		LCC	0.15	0.06	0.08	2		2.88E−05
CH01-LCC2		LCC	0.32	0.04	0.08	4		2.65E−05
CH01-LCC3		LCC	0.15	0.05	0.07	2		3.02E−05
CH01-LCC4		LCC	0.02	0.05	0.08	2		3.19E−05
CH01-LCC5		LCC	−0.26	0.06	0.09	2		3.58E−05
CH01-LCC6		LCC	0.05	0.06	0.09	2		2.76E−05
CH01-LCC7		LCC	0.31	0.05	0.09	3		3.05E−05
CH01-LCC8		LCC	0.10	0.04	0.09	4		2.89E−05
CH01-LCC9		LCC	−0.38	0.06	0.08	2		3.70E−05
CH01-LCC10		LCC	−0.14	0.06	0.08	2		3.52E−05
CH01-100Ac	Summer	SN	0.64	0.07	0.09	2		1.54E−05
CH01-100Av	Summer	SN(N)	0.53	0.04	0.09	5		1.91E−05
CH01-100Bc	Summer	SN	0.56	0.09	0.13	2		1.75E−05
CH01-100Cc	Summer	SNN	0.54	0.12	0.17	2		2.25E−05
CH01-100Dc	Summer	SNN	0.77	0.06	0.09	2		2.67E−05
CH01-100Ec	Summer	SN	0.62	0.07	0.12	3		1.52E−05
CH01-100Ev	Summer	SNN ?	0.32	0.13	0.18	2		1.53E−05
CH01-101Ac	Summer	SN	0.50	0.07	0.12	3		1.36E−05
CH01-101Ec	Summer	SN	0.50	0.07	0.13	3		1.41E−05
CH01-101Epl	Summer	SNN	0.14	0.05	0.08	2		2.14E−05
CH01-102Ac	Summer	SN	0.45	0.06	0.09	2		1.15E−05
CH01-102Bc	Summer	SN	0.36	0.05	0.08	3		1.37E−05
CH01-102Epl	Summer	SNN	0.32	0.04	0.09	5		1.94E−05
CH01-103Ec	Autumn	SN	0.74		0.09	1		1.49E−05
CH01-103F	Autumn	SN	0.42	0.06	0.08	2		1.59E−05
CH01-103G	Autumn	SN	0.39	0.04	0.06	2		1.25E−05
CH01-104Bc	Autumn	SN	0.50	0.06	0.08	2		1.55E−05
CH01-104Cc	Autumn	SN	0.65	0.08	0.11	2		1.57E−05
CH01-104Ec	Autumn	SN	0.51	0.09	0.13	2		1.40E−05
CH01-103Ev	Autumn	SNN	0.55	0.05	0.09	3		1.60E−05
CH01-103Epl	Autumn	SNN	0.63	0.05	0.08	3		1.98E−05
CH01-104Dpl	Autumn	SNN	0.52	0.08	0.12	2		1.59E−05
CH01-104Ev	Autumn	SNN	0.44	0.05	0.09	3		1.69E−05
CH01B-104pl	Autumn	SNN	0.49	0.04	0.09	4		2.87E−05
CH01-104Apl	Autumn	SNO	0.12	0.05	0.07	2		2.31E−05
CH01T-105Dc	Winter	SN	0.75	0.05	0.07	2		1.18E−05
CH01T-105Dv	Winter	SN	0.70	0.06	0.08	2		1.53E−05
CH01-106Epl	Winter	SN	0.50	0.06	0.09	2		2.35E−05
CH01T-106Cc	Winter	SN	0.50	0.07	0.09	2		1.59E−05
CH01T-106Dc	Winter	SN	0.19		0.09	1		1.73E−05
CH01T105Ev	Winter	SNN	0.70	0.06	0.09	2		1.96E−05
CH01T-105Cc	Winter	SN(N)	0.52	0.05	0.08	2		1.86E−05
CH01T-106Dpl	Winter	SNO	0.34	0.06	0.09	2		1.80E−05
CH01IV-106Apl	Winter	SNO	0.15	0.06	0.09	2		2.13E−05
CH01T-105Epl	Winter	SN(N)	0.50	0.05	0.08	2		2.17E−05
CH01T-106Cpl	Winter	SN(N)	0.33	0.06	0.09	2		2.32E−05
CH01T105Apl	Winter	SN(O)	0.33		0.09	1		2.67E−05
CH01-107Ec	Spring	SN	0.29	0.05	0.08	3		1.31E−05
CH01IV-107Ac	Spring	SN	0.37	0.05	0.09	3		2.31E−05
CH01IV-107Bc	Spring	SN	0.38	0.07	0.09	2		1.93E−05
CH01T-108Bc	Spring	SN	0.38	0.06	0.09	2		2.48E−05
CH01T-108Ec	Spring	SN	0.62	0.06	0.08	2		1.66E−05
CH01-107Epl	Spring	SNN	0.47	0.06	0.08	2		2.13E−05
CH01T-107Dpl	Spring	SNN	0.24	0.06	0.09	2		2.31E−05
CH01IV-107Av	Spring	SNN	0.45	0.05	0.07	2		2.35E−05
CH01T-108Epl	Spring	SNN	0.23	0.06	0.11	3		1.94E−05
CH01IV-107Bpl	Spring	SNO	0.34	0.06	0.12	4		2.04E−05
CH01IV-108Bpl	Spring	SNO	0.16	0.11	0.15	2		2.91E−05

[a] For samples analysed once, the average 2 SD is taken as uncertainty. 1 SD of Sr/Ca analyses ≤0.5 %

Thus, it appears that the main sources in Villiers quarry contribute slightly differently to the Sr content of the two pedogenic carbonate phases. This could indicate that different processes are controlling NFC and LCC precipitations.

As explained previously, bulk NFC corresponds to an accumulation of various microscopic morphologies, which can be discriminated into three morphological groups: SN, SNN, and SNO. These microscopic morphologies result from a gradual evolution inside the soil pores: SN

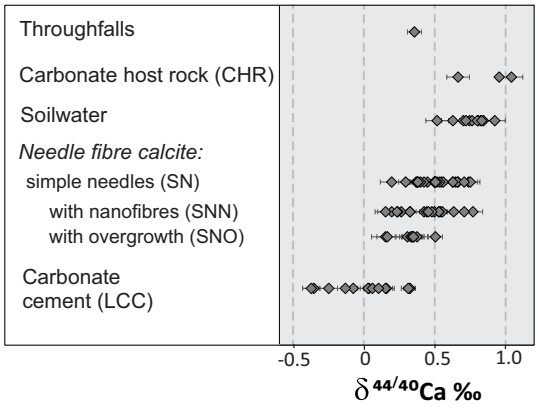

Fig. 5. Plot of the $\delta^{44/40}$Ca ratio values of the different carbonate phases: the three microscopic shapes of needle fibre calcite, i.e. the simple needles (SN), the simple needles with nanofibres (SNN), the simple needles with overgrowths (SNO), as well as the carbonate cement (LCC) and the carbonate host rock (CHR), the surface and deep soil solution (soilwater), and the throughfalls measured at Villiers.

corresponds to the original morphology formed inside fungal hyphae; SNN stands for a combination of simple needles and organic or mineralised nanofibres; and SNO to the formation of calcitic overgrowths along simple needles after their release in soil pores (Verrecchia and Verrecchia, 1994; Cailleau et al., 2009b; Millière et al., 2011a).

The average $^{87}Sr/^{86}Sr$ value of the SN microscopic group is slightly, but significantly, different from the average $^{87}Sr/^{86}Sr$ of SNO and SNN (Table 2, Fig. 4). This difference indicates that the Sr contribution of both sources, i.e. weathering of CHR (carbonate clasts) and weathering of allochthonous minerals, does not contribute in the same proportion to the SN group and the two other micromorphological groups. The Sr isotope signatures of SN are closer to the Sr isotope composition of CHR. Indeed, the calculations show that 85% of Sr and 80% of Ca in SN come from CHR, whereas CHR contributes 81% and 75% of Sr and Ca to SNN and 82% and 76% of Sr and Ca to SNO, respectively. Finally, 78% of Sr and 72% of Ca in LCC come from CHR. While the different contribution of the two main Sr and Ca sources have a significant effect on the $^{87}Sr/^{86}Sr$, the effect on the Ca isotope composition of the respective fluids is limited, because the $\delta^{44/40}$Ca of the CHR is close to bulk silicate earth, which can be assumed to be the composition of the allochthonous compound. A shift of 10% of the CHR contribution therefore leads to an uncertainty in $\delta^{44/40}$Ca, which is lower than the analytical uncertainty.

The different Ca and Sr sources for the different $CaCO_3$ phases might be related to distinct processes contributing to the formation of the morphological groups. As mentioned previously, the SN group is assumed to precipitate directly inside fungal hyphae (Verrecchia and Verrecchia, 1994; Cailleau et al., 2009a; Millière et al., 2011a; Bindschedler et al., 2012). Fungi are present in large amounts in soils and can be categorized with depth regarding their ecology and lifestyle. Saprophytic fungi primarily colonize the litter on the surface of the ground, while mycorrhizal fungi predominate in the underlying and more decayed litter in the mineral horizons (Lindahl et al., 2007). Ectomycorrhizal fungi play an important role at the ecosystem scale in mineral weathering (van Schöll et al., 2008). More precisely, ectomycorrhizal weathering of silicate minerals represents a non-negligible source of Ca in forest ecosystems (e.g. Connolly et al., 1999; Blum et al.,

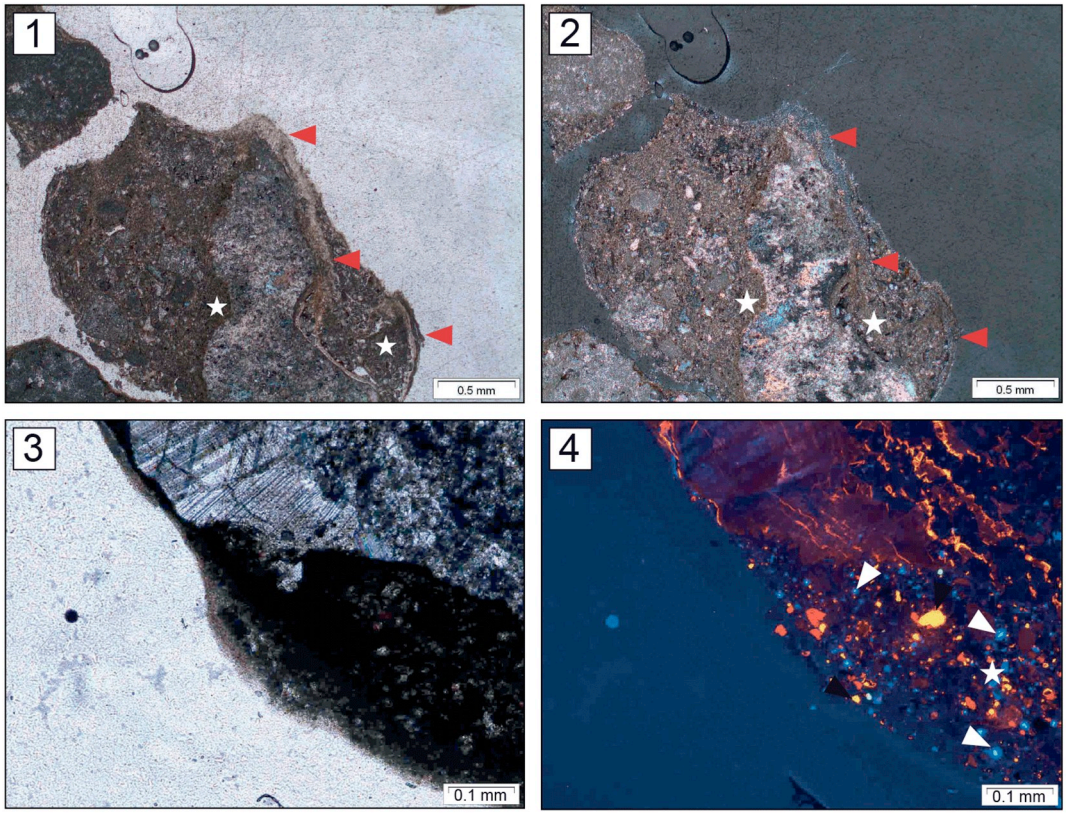

Fig. 6. Micrographs from thin sections of carbonate pebbles sampled in the soil profile showing some fine material accumulation around pebbles (stars), overlapped by a thin layer of NFC (red triangles). (1) Plane polarized light (PPL). (2) Same view in crossed polarized light (XPL). The phenocrysts of calcite from a rock fragment between the stars are colorless in PPL but display high-order colors of birefringence in XPL. (3) Detail in PPL showing calcite phenocrysts of a rock fragment. (4) Same view in cathodoluminescence: quartz is blue (white arrows) and altered grains from the autochthonous limestone appear in bright orange inside a micromass (star). The location of the samples is marked by a bold box in the soil profile at 80 cm deep in Fig. 2. (For interpretation of the references to color in this figure legend, the reader is referred to the web version of this article.)

2002). Since it is impossible to track individual soil-penetrating hyphae, the involvement of fungi other than mycorrhizal fungi in the formation of NFC cannot be excluded. Nevertheless, the fact that NFC has been sampled only in the mineral horizon suggests that mycorrhizal fungi must be principally responsible for the formation of NFC. In addition, some previous studies emphasized the implication of mycorrhizal fungi in the precipitation of calcium carbonate in paleosols (Klappa, 1978; Sanz-Montero and Rodríguez-Aranda, 2012). Mycorrhizal fungi, particularly ectomycorrhizae, have the ability to develop on friable materials in the soil or on rocks by developing a hyphal network, called the mycelium (Carlile et al., 2001; Gadd, 2007). Hyphae may be either isolated or organised into bundles (e.g. fungal stands, rhizomorphs), and follow ridges and grooves of mineral substrates (e.g. Hoffland et al., 2004; Carlile et al., 2001). Ectomycorrhizal fungi are known to be able to penetrate in solid materials by means of both physical and chemical (CO_2 and organic acids) processes in order to release nutrients (Ehrlich, 2002; Gadd, 2007; Bindschedler and Verrecchia, 2019). These nutrients, including Ca and Sr, are transported through the hyphal network, either from the mycelial apex to the host plant or to fungal structures (e.g. survival and reproductive structures) or from these structures to the mycelial front (e.g. Schütte, 1956; Connolly and Jellison, 1997; Landeweert et al., 2001; Carlile et al., 2001). At present, studies on the role of fungi in weathering of minerals and the translocation of nutrients in forest soils, such as at Villiers quarry, are focused on the weathering of silicate minerals by ectomycorrhizal fungi (Landeweert et al., 2001; van Schöll et al., 2008; Courty et al., 2010). For example, Blum et al. (2002) and Wallander et al. (2006) observed the Ca translocation by ectomycorrhizal fungi from silicate minerals in two forest ecosystems by following the $^{87}Sr/^{86}Sr$ ratio. Consequently, ectomycorrhizal processes involved in Ca translocation seem to be the most suited to understand the $^{87}Sr/^{86}Sr$ ratios of three different morphotypes of NFC. The $^{87}Sr/^{86}Sr$ ratio is not modified by ion exchanges, plant uptake, or transportation, allowing the origin of Sr and, by inference, Ca, to be traced accurately (Capo et al., 1998; Åberg et al., 1989; Chen et al., 2012). Wallander et al. (2006) detected traces of ^{87}Sr originating from biotite and microcline in the ectomycorrhizal fungi, demonstrating that they have the potential to transport Sr from minerals to roots. The widespread use of Ca-bearing minerals by fungi suggests that they weather minerals and absorb released ions directly, without ions entering the exchangeable soil medium (Blum et al., 2002). In the context of the Villiers quarry, CHR constitutes a much larger nutrient reservoir than soil allochthonous minerals. Angeles de la Torre et al. (1992) have demonstrated that, even if fungi can degrade phyllosilicates, limestones turn out to be the most affected rock by fungal strains. Thus, it is expected that CHR must be the main source of Ca for fungi in Villiers quarry, even if fungi also dissolve soil allochthonous minerals. A relatively large amount of Ca dissolves during the alteration of CHR, and Ca can be considered as toxic when present in high concentrations (Gadd, 1993). Fungi are able to maintain their internal Ca concentration at a low level, especially by sequestration into their cell wall, on intracytoplasmic proteins, or within organelles, in order to maintain their optimal growth (Jackson and Heath, 1993). In dry environments, pore soil solutions can be highly concentrated in Ca; thus, as it has been suggested for metal-oxalate, it can be postulated that fungi induce the precipitation of Ca-carbonate to decrease the Ca content in the cytoplasm (Whitney, 1989; Gadd, 1999, 2007; Bindschedler et al., 2016). Calcium, as a divalent cation, can bind on polymers present at the inner layer of the hyphal wall with chitin and β glucans. Fungal hyphae have already been mentioned to act as nuclei for crystallisation and attachment of crystals (Went, 1969; Northup and Lavoie, 2001; Gadd, 2007; Bindschedler et al., 2010, 2016). Thus, calcite nuclei can form on proteins or chitin present in the cell wall and grow along the hyphal inner wall, with the hypha acting as a mould. In the case of Villiers quarry, the main part of Ca and Sr constituting the SN calcite crystals appears to originate mainly from the CHR. The precipitation of SN inside the fungal hyphae explains its closer Sr isotope signature to CHR than the other microscopic morphologies, as fungal hyphae directly weather this fraction to access mineral nutrients. The proportion of Sr from soil allochthonous minerals originating from atmospheric dusts in SN (15%) is due to the fact that the fungi must also uptake slight amounts of nutrients from these minerals.

The LCC, SNO, and SNN are enriched in ^{87}Sr compared to the SN, but are together statistically undistinguishable (Table 2). The $^{87}Sr/^{86}Sr$ ratio of the soil solution is higher than CHR, due to the contribution of

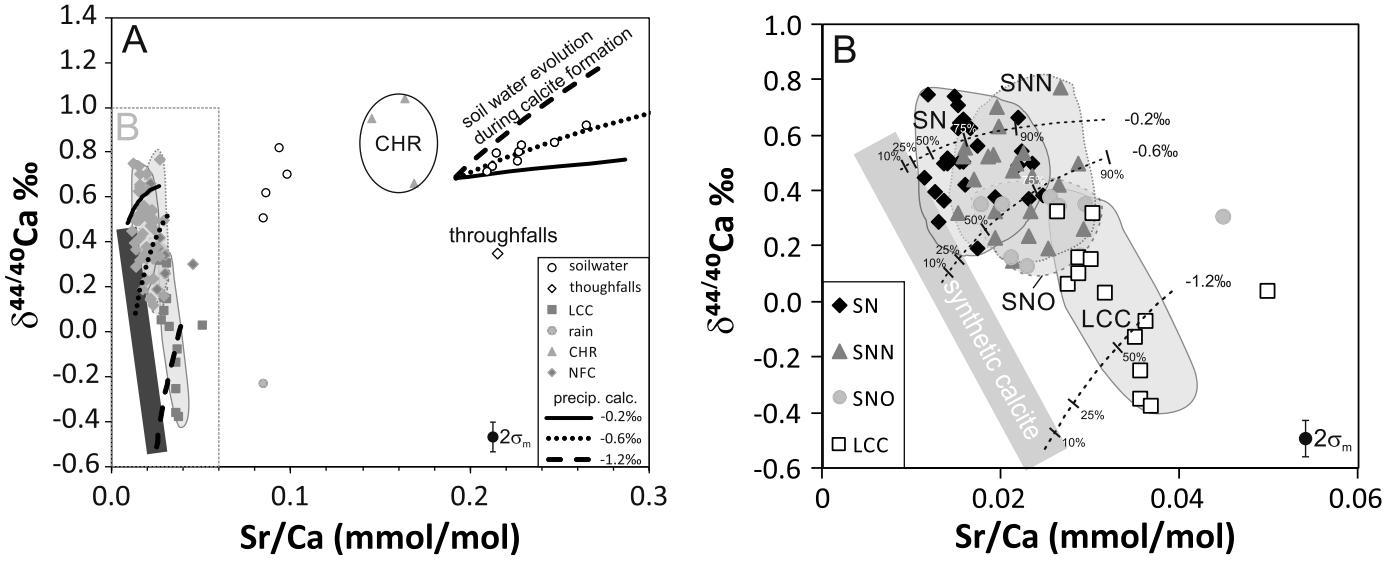

Fig. 7. A: $\delta^{44/40}Ca$ vs Sr/Ca of the carbonate host rock (CHR), late calcite cement (LCC), the three microscopic morphologies of NFC: simple needles (SN), simple needles with nanofibres (SNN), and simple needles with overgrowths (SNO), as well as soil water and throughfalls. The solid, dashed and dotted lines refer to the evolution of calcite and soil water, applying different values for Sr distribution coefficient in calcite and $1000 \cdot Ln(\alpha)$ using the relation for inorganic calcite given by Tang et al. (2008b) at different precipitation rates. As initial fluid composition $\delta^{44/40}Ca$ of 0.65 ‰ and Sr/Ca of $1.9 \cdot 10^{-4}$ were applied, which is intermediate between CHR and throughfalls. B: enlarged detail of A showing the various NFC types (SN, SNN, SNO), LCC, and the domain of the synthetic calcite from Tang et al. (2008b). Dashed, dotted and solid lines represent calculated calcite compositions precipitated from the soil fluid at different precipitation rates, with higher precipitation rates having higher Sr/Ca and lower $\delta^{44/40}Ca$. The ticks indicate the portion of Ca precipitated from a semi enclosed fluid reservoir.

allochthonous minerals during their weathering. The proportion of Ca and Sr originating from soil allochthonous minerals is the most significant in LCC (Ca: 28%; Sr: 22%). This indicates that LCC precipitates directly from the soil solution on calcareous clasts. The rhombohedral overgrowths on the SNO microscopic shapes are assumed to be formed by precipitation along the simple needle, as discussed above (see Cailleau et al., 2009a). Therefore, calcite overgrowths and LCC have the same parent solution and precipitate in similar conditions, explaining their similar Sr isotope signatures. In the SNO group, overgrowths may overprint the Sr isotope signature of SN. The origin of the nanofibres, that are associated to SN in the SNN group, has been thoroughly investigated and attributed to a possible mineralisation of organic nanofibres from plants or hyphal walls (Cailleau et al., 2009b; Bindschedler et al., 2010, 2014). However, the processes leading to the replacement of the organic framework by a crystalline structure are still poorly understood. The study of carbon and oxygen isotope signatures of nanofibres associated to NFC has suggested that carbonate species from the soil solution and some oxidized organic molecules constitute the mineralised nanofibres (Millière et al., 2011a). Both, nanofibres and calcite overgrowths precipitate along simple needles after their release in the soil pores. As a result, the parent solution for LCC and nanofibres of the SNN group is the soil solution. However, nanofibres may be either mineral, and hence have a similar signature that LCC, but they may also be organic. This process can explain the intermediate Sr isotope compositions of SNN, which is between LCC and SN. The Sr isotope data and the contribution of the two main sources of Ca-bearing minerals in the Sr compositions of the different $CaCO_3$ compartments at Villiers quarry are summarized in Fig. 3.

5.3. Calcium isotope compositions and strontium concentrations in carbonate phases at Villiers quarry

Sr/Ca and Ca isotope ratios can be used to shed light on the formation processes of carbonate features, if the composition of their respective parent solutions is well-constrained. In the soil system at Villiers, the throughfall is the only external source of water. By percolating through the first centimetres of soil, throughfall produces the soil surface solution, which develops into the deep soil solution (DSS) by reaching a greater depth in the soil profile. During the course of percolation through the upper horizons enriched in CO_2 and organic acids, soil solutions partly dissolve calcareous clasts inherited from CHR. As a result, Ca isotope compositions and Ca concentrations in soil solutions are intermediate between throughfall and CHR (Tables 1, 3). However, the soil solution samples of both soil inventory and seasonal sampling experiments show two groups in the $\delta^{44/40}$Ca vs. Sr/Ca diagram (Fig. 7). The soil solution sampled during the seasonal sampling experiment follows a trend towards higher Sr/Ca ratios and $\delta^{44/40}$Ca values, while the samples from the first campaign are depleted in Sr relative to Ca, possibly due to partial dissolution of pedogenic calcite (NFC, LCC) prior to or during sampling. Pedogenic $CaCO_3$, namely the three NFC morphotypes and LCC, cluster almost parallel to the fractionation trend of Tang et al. (2008b) for inorganic calcite, with LCC being most enriched in ^{40}Ca and less depleted in Sr, compared to NFC. Within the NFC, the SN shows the heaviest $\delta^{44/40}$Ca and lowest Sr/Ca values, while SNN and SNO are slightly shifted to higher Sr/Ca and/or lower $\delta^{44/40}$Ca. This observation may indicate that the pedogenic $CaCO_3$ form from fluids that are nearly identical or similar with respect to their Sr/Ca ratios and $\delta^{44/40}$Ca values, which is consistent with field observations that the three microscopic shapes of NFC, as well as the LCC, have been found at the same depth in the soil profile.

Besides the fluid composition, several factors influence the Sr/Ca ratios and $\delta^{44/40}$Ca values of $CaCO_3$ minerals. The $\delta^{44/40}$Ca is affected by growth rate (Tang et al., 2008b; Fantle and DePaolo, 2007; DePaolo, 2011; Lemarchand et al., 2004), temperature (Marriott et al., 2004; Gussone et al., 2003), and the Ca^{2+}:CO_3^{2-} stoichiometry of the solution. Nielsen et al. (2012) showed that at high Ca^{2+}:CO_3^{2-} ratios, Ca isotope fractionation is reduced. This process can however not explain the heavy Ca isotope signature found in Villiers quarry, because analyses of soil water [Ca^{2+}] and alkalinity revealed an average Ca^{2+}:CO_3^{2-} ratio of 0.68 ± 0.13, which is even lower compared to the experimental setup by Tang et al. (2008a, 2008b). Consequently, the Ca isotope systematics of Tang et al. (2008a, 2008b) for inorganic calcite can be applied to these pedogenic $CaCO_3$. This would suggest that the relatively small Ca isotope fractionation between the soil solution and NFC morphotypes is likely caused by low precipitation rates, while LCC formed at higher rates.

Moreover, the partitioning of Sr into calcite reveals information on conditions during crystal formation. The incorporation of Sr into calcium carbonate is influenced by the environmental conditions during mineral precipitation and may be used as a proxy to reconstruct physicochemical conditions during calcite formation. The mechanisms of Sr incorporation during calcite formation have been widely studied in biogenic and inorganic calcite (Holland et al., 1964; Lorens, 1981; Tesoriero and Pankow, 1996; Lea et al., 1999; Wasylenki et al., 2005;) demonstrating that precipitation rate, temperature, and biological activity can affect the Sr incorporation. SNO is enriched in Sr compared to SN and SNN morphologies (Table 1), but not as much as in LCC. The variety of NFC morphologies is thought to originate from an initial form (SN) presumed to be physicochemically precipitated inside an organic mould, the fungal hyphae. As described previously, SNO are defined as the accumulation of calcitic overgrowths along SN. Overgrowths are assumed to be formed directly from the soil solution, after the release of SN in the soil pores (Cailleau et al., 2009a, 2009b; Verrecchia and Verrecchia, 1994). According to this hypothesis, the precipitation conditions of overgrowths seem analogous to the precipitation conditions of LCC. Precipitation experiments demonstrated that the Sr/Ca ratio increases in inorganic calcite with precipitation rate (Lorens, 1981; Mucci and Morse, 1983; Huang and Fairchild, 2001; Nehrke et al., 2007; Tang et al., 2008a; Gabitov and Watson, 2006; Gabitov et al., 2014) and in biogenic calcite at a higher growth rate (Lea et al., 1999; Stoll and Schrag, 2000; Stoll et al., 2002a). Previous studies of carbon and oxygen isotope compositions of pedogenic $CaCO_3$ in Villiers quarry have proposed that LCC and NFC (whatever the morphotype) precipitate at similar temperatures (Millière et al., 2011b; Hasinger et al., 2015), and as discussed above, NFC and LCC are formed from similar parent solutions. Thus, it seems that the lower Sr/Ca ratio in SN and SNN than in SNO and LCC can be attributed to a lower calcite growth rate of SN and SNN compared to SNO and LCC. SN are supposed to nucleate on organic molecules in an organic mould, while SNN are assumed to be an association of calcite needles and with mineralised and non-mineralised organic nanofibres (Bindschedler et al., 2010, 2014); consequently, their signature is dominated by the low Sr/Ca ratios measured for SN.

To test the hypothesis whether the pedogenic calcite types can solely be explained by precipitation according to the systematics of Tang et al. (2008a, 2008b), we calculated $\delta^{44/40}$Ca and Sr/Ca evolution curves of soil water and calcite for different Ca isotope fractionation factors (α = 0.9998, 0.9994, 0.9988) and the corresponding Sr/Ca partitioning coefficients according to Tang et al. (2008b) under closed system conditions (Fig. 7). Assuming an initial soil solution of 0.65‰ and 0.19 mmol/mol and 1000 Ln (α) between −0.2 and −1.2‰, the soil solution trend of the seasonal sampling experiment is well explained, and values of pedogenic carbonates as well. Relatively high rates of Ca consumption during $CaCO_3$ precipitation are predicted by the model results, which are however feasible, as precipitation is evaporation controlled, and the Ca:CO_3 ratios < 1 allow for precipitation of large portions of Ca as calcite. This low Ca:CO_3 value is also applicable for the formation within the fungal hyphae. When fungi uptake nutrients from the soil solution, it is likely that large amounts of Ca^{2+} and CO_3^{2-} are concomitantly absorbed, but the inorganic carbon is not metabolized. Therefore, it may be assumed that SN are precipitated as a result of fungal uptake and the concentration of dissolved ions within

hyphal compartments (e.g. vacuoles), until the intrahyphal solution is supersaturated regarding calcite.

According to Tang et al. (2008b), the differences in $\delta^{44/40}$Ca and Sr/Ca of SN and LCC imply slow precipitation rates for the SN and higher rates for the LCC. This observation differs from earlier assumptions that the elongated shape of SN may be related to a high precipitation rate from supersaturated solutions (e.g. Kubiëna, 1938; Vergès et al., 1982; Jones and Ng, 1988). Indeed, in purely physicochemical conditions, rapid growth can induce an elongation of a crystal in one preferred direction, such as the *c*-axis for calcite (Buckley, 1951), thus leading to needle-shaped crystals such as SN. However, the data obtained in this study show that it is more likely that the elongated shape arises from the formation within a constrained biological environment, such as fungal hyphae. Slight chemical changes between the parent solutions allowing precipitation of the various pedogenic $CaCO_3$ in Villiers cannot be totally excluded and may contribute to the variability in Ca isotope and Sr/Ca ratios recorded. The proposed close connection between SN formation and fungi may suggest that the Ca used for SN formation may be affected by the Ca uptake of plants, which preferentially consume light Ca from the soil (e.g. Schmitt et al., 2013). In other words, if this Ca is provided through mycorrhizal fungi, it may be expected that the lighter fraction is transferred to the plant. In the case of Villiers, a clear $\delta^{44/40}$Ca signature for SN compared to SNO and SNN could not be highlighted (Fig. 5). Previous results demonstrated that the distinct microscopic NFC morphologies and LCC precipitate in equilibrium with the dissolved inorganic carbon of the soil solution (Millière et al., 2011a, 2011b; Hasinger et al., 2015) and the Ca-Sr systematics can be explained simply by inorganic precipitation at different rates from a single fluid source.

SN and LCC are both formed at the same time from DSS, but are also impacted by dissolution processes. It is postulated that soil pores act as semi-closed systems between rain events. A first rain event can fill in the soil micro-porosity, and during the following drier period, SN and LCC precipitate from the entrapped solution: SN within the fungal hyphae, and LCC directly in soil pores. Later on, another rain event refills the soil micro-pores, during which SN and LCC may be partly dissolved; such events may have caused the low Sr/Ca ratios of the soil solutions sampled during the soil inventory experiment (Table 1). Then, during the next drier period, calcite overgrowths and crystallisation of nanofibres along SN occurs, leading to SNN and SNO, respectively, along with the formation of new crystals of SN and LCC. This scenario is the most probable, since dissolution and recrystallization of pedogenic carbonate in semi-humid climatic conditions have already been established (e.g. Gocke et al., 2012).

A simple model has been built in order to assess the degree of involvement of the soil solution in the precipitation of the various types of NFC (SN, SNN, SNO) as well as LCC (Fig. 7). The LCC is enriched in ^{40}Ca and Sr compared to NFC, whereas SN crystals are clearly enriched in ^{44}Ca and depleted in Sr compared to LCC. In contrast, LCC are more enriched in ^{40}Ca and less depleted in Sr relative to the soil solution. This suggests that a more rapid precipitation for LCC is likely, while the elongated shape of the SN crystal cannot be related to a rapid precipitation rate, but rather to a slow precipitation under semi-closed conditions, such as in a fungal hypha. In other words, both NFC and LCC are precipitated from the same or a fluid of similar composition, but at different rates. SNN and SNO overlap with the SN, but are, on average, lighter in Ca isotopes and have higher Sr contents. As suggested above, these differences are related to their evolution in the soil environment. SN needles are precipitated within a biological environment (i.e. fungal hyphae), whereas SNO undergo epitactic overgrowths (features close to LCC) in soil pores, giving them intermediate signatures between SN and LCC. Overall, NFC and LCC signatures can be explained by calcite precipitation according to the Sr and Ca systematics of inorganic calcite of Tang et al. (2008b), with different precipitation rates and degrees of Ca and Sr consumptions during precipitation: SN correspond to values of a calcite formed in a semi-restricted environment, supporting the fungal hypothesis for the origin of NFC, whereas LCC are more in agreement with a faster precipitation directly from the soil solution.

6. Conclusions

The study of Sr and Ca isotope compositions and Sr/Ca ratios of three microscopic morphologies of needle-fibre calcite (NFC) and late calcitic cements (LCC) in the context of the Villiers quarry sheds light on the behaviour of Ca in a forest ecosystem under a temperate climate, as well as on the origin and processes leading to the formation of a peculiar pedogenic $CaCO_3$, NFC. At Villiers quarry, soil samples and pedogenic $CaCO_3$ are enriched in ^{87}Sr compared to the carbonate host rock (CHR), indicating the combined influence of allochthonous minerals, related to the successive loess contributions during the Late Pleistocene-Holocene, as well as the present-day dust deposits continuously incorporated in the upper part of the soil. Whereas, Ca and Sr concentrations in soil samples (from 50 cm to 70 cm depth) show the influence of pedogenic $CaCO_3$ formation, with a depletion in Sr while Ca is constant at this depth interval. The Sr isotope signature of the simple needles (SN) is slightly different from the Sr isotope signatures of the simple needle with overgrowths (SNO), simple needle with nanofibres (SNN), and late calcite cement (LCC), indicating that the contribution of the two main Ca sources (CHR and allochthonous deposits) varies in function of the calcite crystal shape. The ^{87}Sr/^{86}Sr ratio of SN is closer to the ^{87}Sr/^{86}Sr ratio of CHR than SNO, SNN, and LCC. Fungi are well known to dissolve rocks, especially limestones, to release and translocate nutrients necessary for their development. Thus, the Sr isotope composition of pedogenic carbonate at Villiers quarry seems to emphasize the affiliation between filamentous fungi and NFC, as already suspected. SN has low Sr/Ca and high $\delta^{44/40}$Ca compared to LCC, while SNN and SNO show intermediate values, between SN and LCC. Finally, the study of Ca isotope compositions of SN, SNN, SNO, and LCC, and their comparison to calculated theoretical values for pedogenic $CaCO_3$ formed in a restricted environment seems to validate that SN is probably formed in a semi-closed system using large portions of available Ca, reinforcing the fungal hypothesis for the origin of SN. Finally, Sr and Ca isotope compositions, as well as Sr/Ca ratios, of the three microscopic NFC morphotypes show that they could correspond to different stages in the formation and evolution of NFC shapes. The clear differences measured between SN and SNO, and to a lesser extent with SNN, emphasize a first step of SN formation within the fungal hyphae, and a second step, when released SN in the soil medium are either overgrown with calcite or associated with nanofibres, which are closer to LCC composition, making both SNO and SNN intermediate between SN and LCC.

Acknowledgements

The authors are grateful to Heidi Bayer and Frank Deipenwisch (University of Münster) for their support in the laboratory, Prof. Igor M. Villa (University of Bern) for his crucial help with measurements of Sr isotopes, and Loïc Liberati (University of Lausanne) for his help with the manuscript. Karin Verrecchia is acknowledged for her careful editing. We thank two anonymous reviewers for their constructive comments and Jerome Gaillardet for the editorial handling. This research has been partly funded by the Swiss National Science Foundation, grants FN 205320-109497 and FN 205320-122171 to EPV and postdoc fellowship PBLAP2-145788 to LM.

References

Åberg, G., Jacks, G., Hamilton, P.J., 1989. Weathering rates and ^{87}Sr/^{86}Sr ratios: an isotopic approach. J. Hydrol. 109, 65–78.

Angeles de la Torre, M., Gomez-Alargon, G., Vizcaino, C., Garcia, M.T., 1992. Biochemical mechanisms of stone alteration carried out by filamentous fungi living in monuments.

Biogeochemistry 19, 129–147.
Arn, R., 1992. Les invasions glaciaires dans la région lémanique. Visions d'hier et d'aujourd'hui. Bulletin de la Société Vaudoise des Sciences Naturelles 78, 21–46.
Atteia, O., 1992. Rôle du sol dans le transfert des éléments traces en solution - application à l'étude de quelques écosystèmes d'altitude (Thèse de doctorat n° 1031). Ecole polytechnique fédérale de Lausanne (Suisse).
Bailey, S.W., Hornbeck, J.W., Driscoll, C.T., Gaudette, H.E., 1996. Calcium inputs and transport in a base-poor forest ecosystem as interpreted by Sr isotopes. Water Resour. Res. 32, 707–719.
Bindschedler, S., Verrecchia, E.P., 2019. Fungal weathering. In: Gargaud, M., Irvine, W.M. (Eds.), Encyclopedia of Astrobiology. Springer (In press).
Bindschedler, S., Millière, L., Cailleau, G., Job, D., Verrecchia, E.P., 2010. Calcitic nanofibres in soils and caves: a putative fungal contribution to carbonatogenesis. Geol. Soc. Lond., Spec. Publ. 336, 225–238.
Bindschedler, S., Millière, L., Cailleau, G., Job, D., Verrecchia, E.P., 2012. An ultrastructural approach to analogies between fungal structures and needle fibre calcite. Geomicrobiol J. 29 (4), 301–313.
Bindschedler, S., Cailleau, G., Braissant, O., Millière, L., Job, D., Verrecchia, E.P., 2014. Unravelling the enigmatic origin of calcitic nanofibres in soils and caves: purely physicochemical or biogenic processes? Biogeosciences 11, 2809–2825.
Bindschedler, S., Cailleau, G., Verrecchia, E.P., 2016. Role of fungi in the biomineralization of calcite. Minerals 6 (41), 1–19. https://doi.org/10.3390/min6020041.
Blum, J.D., Klaue, A., Nezat, C.A., Driscoll, C.T., Johnson, C.E., Siccama, T.G., Eagar, C., Fahey, T.J., Likens, G.E., 2002. Mycorrhizal weathering of apatite as an important calcium source in basepoor forest ecosystems. Nature 417, 729–731.
Blum, J.D., Dasch, A.A., Hamburg, S.P., Yanai, R.D., Arthur, M.A., 2008. Use of foliar Ca/Sr discrimination and $^{87}Sr/^{86}Sr$ ratios to determine soil Ca sources to sugar maple foliage in a northern hardwood forest. Biogeochemistry 87, 287–296.
Borsato, A., Frisia, S., Jones, B., Van der Borg, K., 2000. Calcite moonmilk: crystal morphology and environment of formation in caves in the Italian Alps. J. Sediment. Res. 70, 1171–1182.
Buckley, H.E., 1951. Crystal Growth. (New york, 571p).
Burkhard, M., Sommaruga, A., 1998. Evolution of the western Swiss Molasse basin: structural relations with the Alps and the Jura belt. In: Mascle, A., Puigdefabregas, C., Luterbacher, H.P., Fernandez, M. (Eds.), Cenozoic Foreland Basins of Western Europe. Geological Special Publications, London, pp. 279–298.
Burton, G.R., Rosman, K.J.R., Van de Velde, K.P., Boutron, C.F., 2006. A two century record of strontium isotopes from an ice core drilled at Mt Blanc, France. Earth Planet. Sci. Lett. 248, 217–226.
Cailleau, G., Verrecchia, E.P., Braissant, O., Emmanuel, L., 2009a. The biogenic origin of needle fibre calcite. Sedimentology 56, 1858–1875.
Cailleau, G., Dadras, M., Abolhassani-Dadras, S., Braissant, O., Verrecchia, E.P., 2009b. Evidence for an organic origin of pedogenic calcitic nanofibres. J. Cryst. Growth 311, 2490–2495.
Callot, G., Mousain, D., Plassard, C., 1985a. Concentrations de carbonate de calcium sur les parois des hyphes mycéliens. Agronomie 5, 143–150.
Callot, G., Guyon, A., Mousain, D., 1985b. Inter-relations entre aiguilles de calcite et hyphes mycéliens. Agronomie 5, 209–216.
Cañaveras, J.C., Cuezva, S., Sanchez-Moral, S., Lario, J., Laiz, L., Gonzalez, J.M., Saiz-Jimenez, C., 2006. On the origin of fiber calcite crystals in moonmilk deposits. Naturwissenschaften 93, 27–32.
Capo, R.C., Chadwick, O.A., 1993. Partitioning of atmospheric and silicate weathering sources in the formation of the desert soil carbonate using strontium isotopes. EOS, Transactions, American Geophysical Union 74.
Capo, R.C., Chadwick, O.A., 1999. Sources of strontium and calcium in desert soil and calcrete. Earth Planet. Sci. Lett. 170, 61–72.
Capo, R.C., Stewart, B.W., Chadwick, O.A., 1998. Strontium isotopes as tracers of ecosystem processes: Theory and methods. Geoderma 82, 197–225.
Carlile, M.J., Watkinson, S.C., Dooday, G.W., 2001. The Fungi. Elsevier, London (588 pp).
Chen, S., Lian, B., Zheng, H.Y., Dong, F.Q., 2012. Sr isotope tracing of differences in the effects of microorganisms on weathering of calcite and apatite. Geomicrobiol J. 29 (7), 640–647.
Chiquet, A., Michard, A., Nahon, D., Hamelin, B., 1999. Atmospheric input vs in situ weathering in the genesis of calcretes: an Sr isotope study at Gálvez (Central Spain). Geochim. Cosmochim. Acta 63, 311–323.
Chow, T.J., Bruland, K.W., Bertine, K.K., Soutar, A., Koide, M., Goldberg, E.D., 1973. Records in Southern California coastal sediments. Science 181, 551–552.
Connolly, J.H., Jellison, J., 1997. Two-way translocation of cations by the brown rot fungus Gloeophyllum trabeum. Int. Biodeterior. Biodegradation 39, 181–188.
Connolly, J.H., Shortle, W.C., Jellison, J., 1999. Translocation and incorporation of strontium carbonate derived strontium into calcium oxalate crystals by the wood decay fungus Resinicium bicolor. Can. J. Bot. 77, 179–187.
Courty, P.E., Buéea, M., Gamby Diedhioua, A., Frey-Kletta, P., Le Tacona, F., Rineaua, F., Turpaultd, M.P., Uroz, S., Garbaye, J., 2010. The role of ectomycorrhizal communities in forest ecosystem processes: new perspectives and emerging concepts. Soil Biol. Biochem. 42, 679–698.
Dalla Piazza, R., 1996. Géochimie des altérations dans trois écosystèmes sols tempérés application de l'acquisition des caractéristiques chimiques des solutés (PhD Thesis n° 1483). EPF, Lausanne 364 pp.
De Angelis, M., Gaudichet, A., 1991. Saharan dust deposition over MontBlanc (French Alps) during the last 30 years. Tellus B 43, 61–75.
DePaolo, D.J., 2011. Surface kinetic model for isotopic and trace element fractionation during precipitation of calcite from aqueous solutions. Geochim. Cosmochim. Acta 75 (4), 1039–1056.
Dia, A.N., Cohen, A.S., O'Nions, R.K., Shackleton, N.J., 1992. Seawater Sr isotope variation over the past 300 kyr and influence of global climate cycles. Nature 356, 786–788.
Durand, N., Monger, H.C., Canti, M.G., Verrecchia, E.P., 2018. Calcium carbonate features-chapter 9. In: Stoops, G., Mees, F., Marcelino, V. (Eds.), Interpretation of Micromorphological Features of Soils and Regoliths, 2nd ed. Elsevier, pp. 205–258.
Ehrlich, H.L., 2002. Geomicrobiology. Marcel Dekker, Inc, New York (768pp).
Erel, Y., Patterson, C.C., Scott, M.J., Morgan, J.J., 1990. Transport of industrial lead in snow through soil to stream water and groundwater. Chem. Geol. 85 (3–4), 383–392.
Fantle, M.S., DePaolo, D.J., 2007. Ca isotopes in carbonate sediment and pore fluid from ODP Site 807A: the Ca^{2+}(aq)-calcite equilibrium fractionation factor and calcite recrystallization rates in Pleistocene sediments. Geochim. Cosmochim. Acta 71, 2524–2546.
Gabitov, R.I., Watson, E.B., 2006. Partitioning of strontium between calcite and fluid. Geochemistry Geophysics Geosystems 7, Q11004.
Gabitov, R.I., Sadekov, A., Leinweber, A., 2014. Crystal growth rate effect on Mg/Ca and Sr/Ca partitioning between calcite and fluid: an in situ approach. Chem. Geol. 367, 70–82.
Gadd, G.M., 1993. Interactions of fungi with toxic metals. New Phytol. 124, 25–60.
Gadd, G.M., 1999. Fungal production of citric and oxalic acid: importance in metal speciation, physiology and biogeochemical processes. Adv. Microb. Physiol. 41, 47–92.
Gadd, G.M., 2007. Geomycology: biogeochemical transformations of rocks, minerals, metals and radionuclides by fungi, bioweathering and bioremediation. Mycol. Res. 111, 3–49.
Gocke, M.I., Pustovoytov, P., Kuzyakov, Y., 2012. Pedogenic carbonate formation: recrystallization versus migration - process rates and periods assessed by ^{14}C labelling. Glob. Biogeochem. Cycles 26, GB1018.
Graustein, W.C., Armstrong, R.L., 1983. The use of strontium-87/strontium-86 ratios to measure atmospheric transport into forested watersheds. Science 219, 289–292.
Gussone, N., Friedrich, O., 2018. Cretaceous calcareous dinoflagellate cysts as recorder of $\delta^{44/40}Ca_{seawater}$ and paleo-temperature using Sr/Ca thermometry. Chem. Geol. 488, 138–148.
Gussone, N., Eisenhauer, A., Heuser, A., Dietzel, M., Bock, B., Böhm, F., Spero, H.J., Lea, D.W., Bijma, J., Nägler, T.F., 2003. Model for kinetic effects on calcium isotope fractionation ($\delta^{44}Ca$) in inorganic aragonite and cultured planktonic foraminifera. Geochim. Cosmochim. Acta 67, 1375–1382.
Gussone, N., Böhm, F., Eisenhauer, A., Dietzel, M., Heuser, A., Teichert, B.M.A., Reitner, J., Wörheide, G., Dullo, W.C., 2005. Calcium isotope fractionation in calcite and aragonite. Geochim. Cosmochim. Acta 69, 4485–4494.
Gussone, N., Zonneveld, K., Kuhnert, H., 2010. Minor element and Ca isotope composition of calcareous dinoflagellate cysts of cultured Thoracosphaera heimii. Earth Planet. Sci. Lett. 289 (1–2), 180–188.
Gussone, N., Gernot, N., Teichert, B.M.A., 2011. Calcium isotope fractionation in ikaite and vaterite. Chem. Geol. 285 (1–4), 194–202.
Gussone, N., Schmitt, A.-D., Heuser, A., Wombacher, F., Dietzel, M., Tipper, E., Schiller, M., 2016. Calcium Stable Isotope Geochemistry. Springer Verlag, Berlin, Heidelberg (269 pp).
Hasinger, O., Spangenberg, J., Millière, L., Bindschedler, S., Cailleau, G., Verrecchia, E.P., 2015. Carbon dioxide in scree slope deposits: a pathway from atmosphere to pedogenic carbonate. Geoderma 247-248, 129–139.
Hathorne, E., Gagnon, A., Felis, T., Adkins, J., Asami, R., Boer, W., Caillon, N., Case, D., Cobb, K., Douville, E., deMenocal, P., Eisenhauer, A., Garbe-Schönberg, D., Geibert, W., Goldstein, S., Hughen, K.A., Inoue, M., Kawahata, H., Kölling, M., Le Cornec, F., Linsley, B., McGregor, H., Montagna, P., Nurhati, I., Quinn, T., Raddatz, J., Rebaubier, H., Robinson, H., Sadekov, A., Sherrell, R., Sinclair, D., Tudhope, S., Wei, G., Wong, H., Wu, H., You, C.-F., 2013. Inter-laboratory study for coral Sr/Ca and other element/Ca ratio measurements. Geochem. Geophys. Geosyst. https://doi.org/10.1002/ggge.20230.
Heuser, A., Eisenhauer, A., Gussone, N., Bock, B., Hansen, B.T., Nägler, T.F., 2002. Measurement of calcium isotopes ($\delta^{44}Ca$) using a multicollector TIMS technique. Int. J. Mass Spectrom. 220, 385–397.
Heuser, A., Schmitt, A.-D., Gussone, N., Wombacher, F., 2016. Analytical methods. 2016 In: Gussone, N., Schmitt, A.-D., Heuser, A., Wombacher, F., Dietzel, M., Tipper, E., Schiller, M. (Eds.), Calcium Stable Isotope Geochemistry. Springer, Heidelberg (260pp).
Hoffland, E., Kuyper, T.W., Wallander, H., Plassard, C., Gorbushina, A.A., Haselwandter, K., Holmström, S., Landeweert, R., Lundström, U.S., Rosling, A., Sen, R., Smits, M.M., van Hees, P.A., van Breemen, N., 2004. The role of fungi in weathering. Front. Ecol. Environ. 2, 258–264.
Holland, H.D., Holland, H.J., Munoz, J.L., 1964. The coprecipitation of cations with CaCO3-II. The coprecipitation of Sr^{2+} with calcite between 90 and 100 °C. Geochim. Cosmochim. Acta 28, 1287–1301.
Huang, Y., Fairchild, I.J., 2001. Partitioning of Sr^{2+} and Mg^{2+} into calcite under karst-analogue experimental conditions. Geochim. Cosmochim. Acta 65, 47–62.
Humphrey, J.D., Howell, R.P., 1999. Effect of differential stress on strontium partitioning in calcite. Journal of Sedimentary 69, 208–215.
IUSS Working Group WRB, 2006. World reference base for soil resources 2006. In: Food and Agriculture Organization of the United Nations. World Soil Resources Reports No. 103 FAO, Rome (145 pp).
Iwanoff, L.L., 1906. Ein wasserhaltiges calcium carbonat aussen umgebung von Nowo-Alexandria (guv. Lublin). Annalen der Geologie und Mineralogie der Russland 8, 23–25.
Jackson, S.L., Heath, I.B., 1993. Roles of calcium ions in hyphal tip growth. Microbiol. Mol. Biol. Rev. 57 (2), 367–382.
Jones, B., Kahle, C.F., 1993. Morphology, relationship, and origin of fiber and dendrite calcite crystals. J. Sediment. Petrol. 63, 1018–1031.
Jones, B., Ng, K.C., 1988. The structure and diagenesis of rhizoliths from Cayman Brac,

Brittish West Indies. J. Sediment. Petrol. 58, 457–467.
Jouaffre, D., 1989. Pédogenèse et rubéfaction post-würmienne en climat montagnard humide (Jura) (Thèse doct.). Univ. Franche-Comté, Besançon (277 pp.).
Katz, A., Sass, E., Starinsky, A., Holland, H.D., 1972. Strontium behavior in the aragonite-calcite transformation: an experimental study at 40–98 °C. Geochim. Cosmochim. Acta 36, 481–496.
Kinsman, D.J.J., 1969. Interpretation of Sr^{2+} concentrations in carbonate minerals and rocks. J. Sediment. Petrol. 39, 486–508.
Klappa, C.P., 1978. Biolithogenesis of microdium: elucidation. Sedimentology 25, 489–522.
Kubiëna, W.L., 1938. Micropedology. Collegiate Press, Ames, Iowa (243 pp.).
Landeweert, R., Hoffland, E., Finlay, R.D., Kuyper, T.W., Van Breemen, N., 2001. Linking plants to rocks: ectomycorrhizal fungi mobilize nutrients from minerals. Trends Ecol. Evol. 1, 248–254.
Langer, G., Gussone, N., Nehrke, G., Riebesell, U., Eisenhauer, A., Kuhnert, H., Rost, B., Trimborn, S., Thoms, S., 2006. Coccolith strontium to calcium ratios in Emiliania huxleyi: the dependence on seawater strontium and calcium concentrations. Limnol. Oceanogr. 51, 310–320.
Lea, D.W., Mashiotta, T.A., Spero, H.J., 1999. Controls on magnesium and strontium uptake in planktonic foraminifera determined by live culturing. Geochim. Cosmochim. Acta 63, 2369–2379.
Lemarchand, D., Wasserburg, G.J., Papanastassiou, D.A., 2004. Rate-controlled calcium isotope fractionation in synthetic calcite. Geochim. Cosmochim. Acta 68, 4665–4678.
Li, G., Chen, J., Chen, Y., 2013. Primary and secondary carbonate in Chinese loess discriminated by trace element composition. Geochim. Cosmochim. Acta 103, 26–35.
Li, T., Liu, F., Abels, H.A., You, C.-F., Zhang, Z., Chen, J., Ji, J., Li, L., Li, L., Liu, H.-C., Ren, C., Xia, R., Zhao, L., Zhang, W., Li, G., 2017. Continued obliquity pacing of East Asian summer precipitation after the mid-Pleistocene transition. Earth Planet. Sci. Lett. 457, 181–190.
Lindahl, B., Ihrmark, K., Boberg, J., Trumbore, S.E., Högberg, P., Stenlid, J., Finlay, R.D., 2007. Spatial separation of litter decomposition and mycorrhizal nitrogen uptake in a boreal forest. New Phytol. 173, 611–620.
Lorens, R.B., 1981. Sr, Cd, Mn and Co distribution coefficients in calcite as a function of calcite precipitation rate. Geochim. Cosmochim. Acta 45, 553–561.
Malone, M.J., Baker, P.A., 1999. Temperature dependence of the strontium distribution coefficient in calcite: an experimental study from 40° to 200 °C and application to natural diagenetic calcites. J. Sediment. Res. 69, 216–223.
Marriott, C.S., Henderson, G.M., Belshaw, N.S., Tudhope, A.W., 2004. Temperature dependence of δ^7Li, δ^{44}Ca and Li/Ca during growth of calcium carbonate. Earth Planet. Sci. Lett. 222, 615–624.
Martignier, L., Verrecchia, E.P., 2013. Weathering processes in superficial deposits (regolith) and their influence on pedogenesis: a case study in the Swiss Jura Mountains. Geomorphology 189, 26–40.
Martignier, L., Adatte, T., Verrecchia, E.P., 2013. Bedrock versus superficial deposits in the Swiss Jura Mountains: what is the legitimate soil parent material? Earth Surf. Process. Landf. 38, 331–345.
Martignier, L., Nussbaumer, M., Adatte, T., Gobat, J.-M., Verrecchia, E.P., 2015. Assessment of a locally-sourced loess system in Europe: the Swiss Jura Mountains. Aeolian Res. 18, 11–21.
McIntire, W.L., 1963. Trace element partition coefficients-a review of theory and applications to geology. Geochim. Cosmochim. Acta 27, 1209–1264.
Meyer, K., 1991. Bodenverschmutzung in der Schweiz. Themenbericht. Ed. Nationales Forschungsprogramm No. 22 “Boden”. (Liebefeld, Bern, 240 pp).
Middleton, N.J., Goudie, A.S., 2001. Saharan dust: sources and trajectories. Trans. Inst. Br. Geogr. 26, 165–181.
Miller, J.D., Cooper, J.M., Miller, H.G., 1993. Acomparison of above-ground component weights and element amounts in four species at KirktonGlen. J. Hydrol. 145, 419–438.
Millière, L., Hasinger, O., Bindschedler, S., Cailleau, G., Spangenberg, J.E., Verrecchia, E.P., 2011a. Stable carbon and oxygen isotope signature of pedogenic needle fibre calcite: further insight into its origin and relationship with soil conditions. Geoderma 161, 74–87.
Millière, L., Spangenberg, J.E., Bindschedler, S., Cailleau, G., Verrecchia, E.P., 2011b. Reliability of stable carbon and oxygen isotope compositions of pedogenic needle fibre calcite as environmental indicators: examples from Western Europe. Isot. Environ. Health Stud. 47, 341–358.
Morse, J.W., Bender, M.L., 1990. Partition coefficients in calcite: examination of factors influencing the validity of experimental results and their application to natural systems. Chem. Geol. 82, 265–277.
Moynier, F., Fujii, T., 2017. Calcium isotope fractionation between aqueous compounds relevant to low-temperature geochemistry, biology and medicine. Sci. Rep. 7, 44255. https://doi.org/10.1038/srep44255.
Mucci, A., Morse, J.W., 1983. The incorporation of Mg^{2+} and Sr^{2+} into calcite overgrowths: influences of growth rate and solution composition. Geochim. Cosmochim. Acta 47, 217–233.
Mügge, O., 1914. Über die lublinit genannte, augeblich neue Modification des kohlensauren Kalkes. Zentralblatt für Mineralogie, Geologie, und Palaontologie 673–675.
Naiman, Z., Quade, J., Patchett, P.J., 2000. Isotopic evidence for aeolian recycling of pedogenic carbonate and variations in carbonate dust sources throughout the southwest United States. Geochim. Cosmochim. Acta 64, 3099–3109.
Nakano, T., Jeon, S.R., Shindo, J., Fumoto, T., Okada, N., Shimada, J., 2001. Sr isotopic signature in plant-derived Ca in rain. Water Air Soil Pollut. 130, 769–774.
Négrel, P., Roy, S., 1998. Chemistry of rainwater in the Massif Central (France): a strontium isotope and major element study. Appl. Geochem. 13, 941–952.
Nehrke, G., Reichart, G.J., Van Cappellen, P., Meile, C., Bijma, J., 2007. Dependence of calcite growth rate and Sr partitioning on solution stoichiometry: non-Kossel crystal growth. Geochim. Cosmochim. Acta 71, 2240–2249.
Ng, A., Patterson, C.C., 1982. Changes of lead and barium with time in California offshore basin sediments. Geochim. Cosmochim. Acta 46 (11), 2307–2321.
Nielsen, L.C., DePaolo, D.J., De Yoreo, J.J., 2012. Self-consistent ion-by-ion growth model for kinetic isotopic fractionation during calcite precipitation. Geochim. Cosmochim. Acta 86, 166–181.
Nielsen, L.C., De Yoreo, J.J., DePaolo, D.J., 2013. General model for calcite growth kinetics in the presence of impurity ions. Geochim. Cosmochim. Acta 115, 100–114.
Northup, D.E., Lavoie, K.H., 2001. Geomicrobiology of caves: a review. Geomicrobiol J. 18, 199–222.
Ockert, C., Gussone, N., Kaufhold, S., Teichert, B.M.A., 2013. Isotope fractionation during Ca exchange on clay minerals in a marine environment. Geochim. Cosmochim. Acta 112, 374–388.
Okai, T., Suzuki, A., Kawahata, H., Terashima, S., Imai, N., 2004. Preparation of a new geological survey of Japan geochemical reference material: coral JCp-1. Geostand. Newslett. 26, 95–99.
Pfeifer, H.-R., Lavanchy, J.-C., Serneels, V., 1991. Bulk chemical analysis of geological and industrial materials by X-ray fluorescence, recent developments and application to material rich in iron oxide. Journal Trace Microprobe Technique 9, 127–147.
Phillips, S.E., Self, P.G., 1987. Morphology, crystallography and origin of needle fiber calcite in quaternary pedogenic calcretes of South Australia. Aust. J. Soil Res. 25, 429–444.
Pochon, M., 1978. Origine et évolution des sols du Haut-Jura suisse. Phénomènes d'altération des roches calcaires sous climat tempéré humide. Mémoires de la Société Helvétique des Sciences Naturellespp. 190.
Poszwa, A., Dambrine, E., Pollier, B., Atteia, O., 2000. A comparison between Ca and Sr cycling in forest ecosystems. Plant Soil 225, 299–310.
Pourcelot, L., Stille, P., Aubert, D., Solovitch-Vella, N., Gauthier-Lafaye, F., 2008. Comparative behaviour of recently deposited radiostrontium and atmospheric common strontium in soils (Vosges mountains, France). Appl. Geochem. 23, 2880–2887.
Quade, J., Chivas, A.R., McCulloch, M.T., 1995. Strontium and carbon isotope tracers and the origins of soil carbonate in South Australia and Victoria. Palaeogeogr. Palaeoclimatol. Palaeoecol. 113, 103–117.
Sanz-Montero, M.E., Rodríguez-Aranda, J.P., 2012. Endomycorrhizae in Miocene paleosols: implications in biotite weathering and accumulation of dolomite in plant roots (SW Madrid Basin, Spain). Palaeogeogr. Palaeoclimatol. Palaeoecol. 333-334, 121–130.
Schmitt, A.-D., Stille, P., 2005. The source of calcium in wet atmospheric deposits: Ca-Sr isotope evidence. Geochim. Cosmochim. Acta 69, 3463–3468.
Schmitt, A.-D., Cobert, F., Bourgeade, P., Ertlin, D., Labolle, F., Gangloff, S., Badot, P.-M., Chabaux, F., Stille, P., 2013. Calcium isotope fractionation during plant growth under a limiting nutrient supply. Geochim. Cosmochim. Acta 110, 70–83.
Schmitt, A.-D., Borrelli, N., Ertlen, D., Gangloff, S., Chabaux, F., Osterrieth, M., 2018. Stable calcium isotope speciation and calcium oxalate production within beech tree (Fagus sylvatica L.) organs. Biogeochemistry 137, 197–217.
van Schöll, L., Kuyper, T.W., Smits, M.M., Landeweert, R., Hoffland, E., van Breemen, N., 2008. Rock-eating mycorrhizas: their role in plant nutrition and biogeochemical cycles. Plant Soil 303, 35–47.
Schultz, J.P., Jarrett, A.R., Hoover, J.R., 1985. Detachment and splash of a cohesive soil by rainfall. American Society of Agricultural and Biological Engineers 28, 1878–1884.
Schütte, K.H., 1956. Translocation in the fungi. New Phytol. 55, 164–182.
Schwikowski, M., Seibert, P., Baltensperger, U., Gäggeler, H.W., 1995. A study of an outstanding Saharan dust event at the high-alpine site Jungfraujoch, Switzerland. Atmos. Environ. 29, 1829–1842.
Shirahata, H., Elias, R.W., Patterson, C.C., 1980. Chronological variations in concentrations and isotopic compositions of anthropogenic atmospheric lead in sediments of a remote subalpine pond. Geochimica Cosmochimica Acta 44, 149–162.
Steinmann, M., Stille, P., 1997. Rare earth element behavior and Pb, Sr, Nd isotope systematics in a heavy metal contaminated soil. Appl. Geochem. 12, 607–623.
Stoll, H.M., Schrag, D.P., 2000. Coccolith Sr/Ca as a new indicator of coccolithophorid calcification and growth rate. Geochemistry Geophysics Geosystems 1 (5), 1–24.
Stoll, H.M., Klaas, C.M., Probert, I., Ruiz Encinar, J., Garcia Alonso, J.I., 2002a. Calcification rate and temperature effects on Sr partitioning in coccoliths of multiple species of coccolithophorids in culture. Glob. Planet. Chang. 34, 153–171.
Stoll, H.M., Rosenthal, Y., Falkowski, P., 2002b. Climate proxies from Sr/Ca of coccolith calcite: calibrations from continuous culture of Emiliania huxleyi. Geochim. Cosmochim. Acta 66, 927–936.
Stoops, G.J., 1976. On the nature of «lublinite» from Hollanta (Turkey). Am. Mineral. 61, 172.
Tang, J., Köhler, S.J., Dietzel, M., 2008a. Sr^{2+}/Ca^{2+} and $^{44}Ca/^{40}Ca$ fractionation during inorganic calcite formation: I. Sr incorporation. Geochim. Cosmochim. Acta 72, 3718–3732.
Tang, J., Dietzel, M., Böhm, F., Köhler, S.J., Eisenhauer, A., 2008b. Sr^{2+}/Ca^{2+} and $^{44}Ca/^{40}Ca$ fractionation during inorganic calcite formation: II. Ca isotopes. Geochim. Cosmochim. Acta 72, 3733–3745.
Teichert, B.M.A., Gussone, N., Eisenhauer, A., Bohrmann, G., 2005. Clathrites: Archives of near-seafloor pore-fluid evolution ($\delta^{44/40}$Ca, δ^{13}C, δ^{18}O) in gas hydrate environments. Geology 33, 213–216.
Teichert, B.M.A., Gussone, N., Torres, M.E., 2009. Controls on calcium isotope fractionation in sedimentary porewaters. Earth Planet. Sci. Lett. 279, 373–382.
Tesoriero, A.J., Pankow, J.F., 1996. Solid solution partitioning of Sr^{2+}, Ba^{2+}, and Cd^{2+} to calcite. Geochim. Cosmochim. Acta 60, 1053–1063.
Van der Hoven, S.J., Quade, J., 2002. Tracing spatial and temporal variations in the sources of calcium in pedogenic carbonates in a semiarid environment. Geoderma

108, 259–276.
Vergès, V., Madon, M., Bruand, A., Bocquier, G., 1982. Morphologie et cristallogenèse de microcristaux supergènes de calcite en aiguille. Bulletin minéralogique 105, 351–356.
Verrecchia, E.P., Verrecchia, K.E., 1994. Needle-fiber calcite: a critical review and proposed classification. J. Sediment. Res. 64, 650–664.
Waight, T., Baker, J., Peate, D., 2002. Sr isotope ratio measurements by double-focusing MC-ICPMS: techniques, observations and pitfalls. Int. J. Mass Spectrom. 221, 229–244.
Wallander, H., Hagerberg, D., Åberg, G., 2006. Uptake of ^{87}Sr from microcline and biotite by ectomycorrhizal fungi in a Norway spruce forest. Soil Biol. Biochem. 38, 2487–2490.
Wasylenki, L.E., Dove, P.M., Wilson, D.S., De Yoreo, J.J., 2005. Nanoscale effects of strontium on calcite growth: an in situ AFM study in the absence of vital effects. Geochim. Cosmochim. Acta 69, 3017–3027.
Went, F.W., 1969. Fungi associated with stalactite growth. Science 166, 385–386.
Whitney, K.D., 1989. Systems of biomineralization in the fungi. In: Crick, R.E. (Ed.), Origin, Evolution and Modern Aspects of Biomineralization in Plants and Animals. Plenum Press, New York, pp. 433–444.